Shear Induced Morphology of Semicrystalline Block Copolymers

by

Peter Kofinas

S.B., Chemical Engineering
Massachusetts Institute of Technology, 1989
S.M., Chemical Engineering Practice
Massachusetts Institute of Technology, 1989

Submitted to the Department of Materials Science and Engineering
Program in Polymer Science and Technology
in partial fulfillment of the requirements for the degree of

Doctor of Philosophy

at the

MASSACHUSETTS INSTITUTE OF TECHNOLOGY

May 1994

Author ....
Department of Materials Science and Engineering
Program in Polymer Science and Technology
April 29, 1994

Certified by ....
Robert E. Cohen
Miles Professor of Chemical Engineering
Thesis Supervisor

Accepted by ....
Carl V. Thompson II
Professor of Electronic Materials
Chair, Departmental Committee on Graduate Students

Shear Induced Morphology of Semicrystalline Block Copolymers

by

Peter Kofinas

Submitted to the Department of Materials Science and Engineering
Program in Polymer Science and Technology
on April 29, 1994, in partial fulfillment of the
requirements for the degree of
Doctor of Philosophy

Abstract

A series of semicrystalline diblock and triblock copolymers of poly(ethylene) (E) and poly(ethylene - propylene) (EP) were subjected to high levels of plane strain compression using a channel die. Deformations were imposed both below and above the melting point of the ethylene block. The lattice unit cell orientation of the crystallized E chains with respect to the lamellar superstructure was determined, as well as the lamellar orientation relative to the specimen boundaries using wide-angle X-ray diffraction pole figure analysis and two dimensional small-angle X-ray scattering. When the diblocks are textured above the E block melting point at various compression ratios, the lamellae orient perpendicular to the plane of shear, while texturing below T_m causes the lamellae to orient parallel to the plane of shear. The triblocks exhibit either lamellar orientation when textured above the E block melting point depending on the applied stress on the channel die during deformation. The orientation of the crystallized E chains for all the polymer systems was perpendicular to the lamellar normal, irrespective of the texturing temperature. Gas permeability coefficients P for several gases (He, CO_2, CH_4, O_2) were measured at 25 °C for the randomly oriented diblocks, and a simple model was presented describing the gas transport in these polymer systems. It predicts the permeability of a randomly oriented spherulitic diblock specimen from the values of the permeability coefficients of the individual lamellar regions of the copolymer. Model predictions were in excellent agreement with the experimental data. The upper bound (lamellae aligned in parallel with respect to the permeation direction) and lower bound (series lamellar alignment) models were calculated and compared to a limited amount of corresponding experimental data on oriented diblock and triblock specimens.

Thesis Supervisor: Robert E. Cohen
Title: Miles Professor of Chemical Engineering

Acknowledgments

There are no words that can truly express my gratitude to my advisor, Professor Robert E. Cohen, for whom I've worked for nine years, since undergraduate freshman orientation week at MIT. His continuous encouragement, exceptional guidance and advice over the years have helped me shape my carreer path. He has been like a father to me, listening to all my problems, always being supportive and bearing my mood swings. I will always hold him as a role model for everything I wish to accomplish in the future.

Contents

List of Figures

List of Tables

Chapter 1

Introduction

The use of polymers in gas transport applications is constantly increasing [1, 2]. Their most prominent use is in membranes for gas separations, due to the low energy requirements for membrane processes compared to other conventional separation techniques [3]. The replacement of conventional glass and metal packagings in grocery stores with polymeric materials in the recent years is the most dramatic evidence of their expanding use in the food and packaging industry [2].

Control over gas transport is essential to the development of polymer membranes for gas separation and barrier material applications. These goals can be achieved with heterogeneous polymer systems, which can be used to design membranes having the structural characteristics of one component and the permeability characteristics of the other. For the case of heterogeneous block copolymers, the features in these systems which affect gas transport are the size, shape and orientation of the microphase separated morphology, the high internal surface-to-volume ratio, and the diffuse interfacial regions.

In previous investigations from this laboratory on gas permeability (P) of a poly (styrene) / poly (butadiene) diblock copolymer with a lamellar morphology, alternating lamellae of polystyrene (PS) and polybutadiene (PB) were either misordered [4], aligned in parallel (high P) [5], or in series [6] (low P) with respect to the permeation direction. A simple model was proposed to describe gas transport in this amorphous polymer system [4].

Recently, more and more interest is being directed toward the study of semicrystalline block polymers. These materials offer a much wider range of possibilities with regards to increased toughening, resistance to solvents and acids and higher working temperature applications. Along with these advantages, incorporating crystallinity into a new material also presents a variety of challenging problems both from a synthesis and a processing point of view. The synthetic pathways required to produce semicrystalline block copolymers are generally more complex than for wholly amorphous systems, and interaction between the kinetically driven crystallization process and the thermodynamically driven phase separation has become a topic of several research efforts.

Work in this laboratory on semicrystalline diblock copolymers [7, 8] determined the lattice unit cell orientation with respect to the lamellar microstructure for diblock copolymers containing a crystallizable ethylene block. The orientation of the crystallized ethylene chains was found to be perpendicular to the lamellar normals. This unusual chain alignment was attributed to the influence of interface - dominated nucleation and topological constraints on growth when the ethylene block chains crystallize within the amorphous lamellar microdomains present in the heterogeneous melt phase of the block copolymers. Bates and co-workers [9, 10, 11] have studied the lamellar orientation of nearly symmetric amorphous poly (ethylethylene) / poly (ethylene-propylene) (EE/EP) diblock copolymer samples, which were textured using large strain dynamic shear. Near the order-disorder transition (ODT) temperature, and at low shear frequencies, the lamellae arrange parallel to the plane of shear, while higher frequency processing leads to lamellae perpendicular to the plane of shear. At temperatures further below the ODT the parallel lamellar orientation is obtained at all shearing frequencies.

These interesting and unexpected results was the motivation for the present research effort to enquire into the possibility that semicrystalline block copolymer systems might also exhibit the perpendicular lamellar morphology under shear, and that the various morphologies exhibited under shear can be used as model systems for gas transport control applications.

The lamellar orientation and chain organization upon crystallization for various processing histories near the ODT and below the crystallization temperature was determined, in a series of diblock and triblock copolymers having crystalline quasi-poly (ethylene) (E) blocks and amorphous poly (ethylene-propylene) (EP) blocks. Mechanical properties of E/EP diblocks and E/EP/E triblocks have been reported [12, 13], and some work has been done to characterize the morphology on the length scale of microdomains [13, 14]. There has been, however, no study of gas transport through these semicrystalline materials or on the morphologies exhibited under an imposed shear field.

The results presented in this thesis will demonstrate that changes in the temperature of plane strain compression processing can be used to force the lamellae to orient either perpendicular or parallel to the plane of shear; the orientation of the crystallized E chains, however, always remains parallel to the plane of the lamellar superstructure irrespective of the processing temperature. It will also be shown that the same simple model that described the permeation of gases through the PS/PB system also applies to the E/EP polymers, even though the crystallization of the E blocks provides added degrees of morphological complexity in the E/EP materials.

The unusual shear-induced lamellar morphologies exhibited in the E/EP and E/EP/E systems may have some potential advantages; for example, a 'parallel' material can be constructed from the perspective of high flux transport through a film. The structure in which the alternating amorphous and semicrystalline lamellae are oriented normal to the film surfaces enables the membrane designer to enjoy the structural and thermal stability offered by the semicrystalline regions without having them interfere with the gas flux through the amorphous lamellae. The 'series' material, having its lamellae oriented parallel to the film surface, would represent the limiting case for a good barrier membrane.

Chapter 2

Theoretical considerations

2.1 Microphase separation in amorphous block copolymers

Block copolymers are a specific class of macromolecules where the monomer units are arranged into long sequences of a particular monomer type within a single chain. Two or three of these long sequences, called 'blocks', are covalently bonded together to produce diblock or triblock copolymers.

The microphase behavior of wholly amorphous A-B diblock copolymers is now generally understood. They can undergo an *order-disorder transition*(ODT), frequently referred to as the *microphase separation transition* (MST), as well as a number of order-order transitions. At temperatures below T_{ODT} the block copolymers form highly ordered morphologies with spatially periodic composition fluctuations (domains), while above T_{ODT}, the copolymer molecules are randomly mixed in a disordered state. Four ordered microphases are well known (Figure 2-1), which consist of alternating lamellae (L), cylinders on a hexagonal lattice (C), spheres on a body centered cubic lattice (S), and a bicontinuous 'double-diamond' structure (OBDD) [15, 16]. In the strong segregation regime, i.e. far from the ODT, the equilibrium phases are believed to depend only on the volume fraction of one of the blocks. The behavior in weak segregation appears to be more complicated, with other additional

Figure 2-1: Block copolymer morphologies

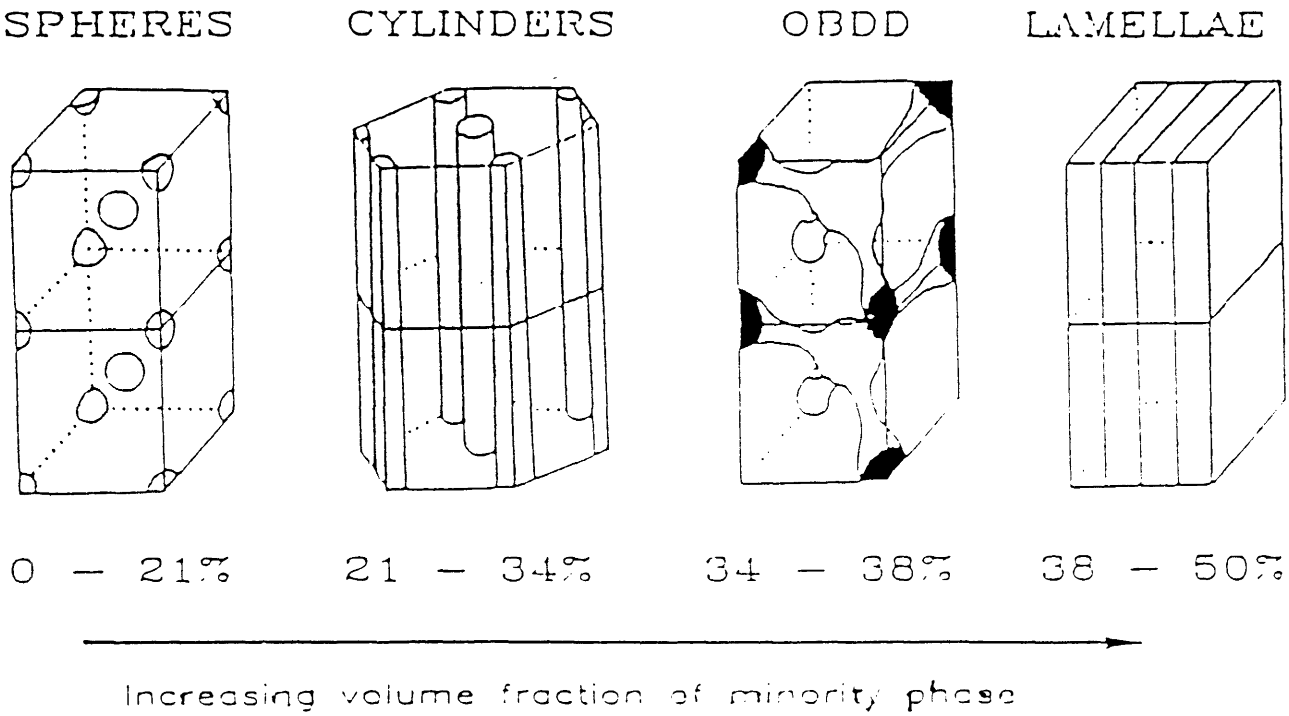

phases becoming stable near the ODT [9, 17]. Block copolymer phase transitions are weakly first order [18]. Roe et al [19] and Hashimoto et al [20, 21] were the first groups to use SAXS techniques to observe structural changes in amorphous block copolymers near the ODT. Since then, many research groups have studied the ODT in amorphous block copolymers using SAXS and rheology [11, 22, 23].

One of the most attractive characteristics of block copolymers is the targeting of well defined equilibrium morphologies that can be achieved in these systems. Morphology control is one of the most important research subjects, since the mechanical properties of the block copolymers depend strongly on their structures. The kind of microphase-separated morphology that will be exhibited depends on the volume fraction of the components comprising the blocks, the molecular weight of the copolymer, and the segmental interactions between the different components of the copolymer [24]. The size scale of the microdomains depends upon the minimization of the free energy which contains contributions from, among other things, the energy required to stretch the chains of each block at the interface so as to minimize contacts between the two different blocks. The extent to which chains are stretched at the interface will dictate the variation in the periodicity of the microdomain morphology.

2.2 Theories on phase transitions in block copolymer melts

Helfand et al.[25, 26, 27, 28] have developed a statistical thermodynamic theory for microdomain structures of block copolymers. According to this theory, it is possible to expect equilibrium domain sizes for respective morphologies with a given set of molecular weight and composition. It also allows the prediction of the equilibrium morphology in the strong segregation limit. Their model is derived from an assumption that the configurational statistics of the component chains reflected Gaussian behavior in the melt.

Their resulting free energy consists of a linear decomposition of the total free energy into potentials arising from the formation of domains, the creation of surfaces between these domains, and junction point fluctuations within the interface region. The linear decomposition of the total free energy is justified by the narrow interface approximation (NIA). This assumption states that the domains are well defined, exhibiting sharp interfaces, a feature which is expected only in the strong segregation limit. The formulation of the theory contains a self-consistent solution of the diffusion equation for the partition function [25]. The free energy, in terms of the partition function, is given as a function of the quench parameter χN, the fractional length of the A block, $f(f = N_A/N$ where N_A is the degree of polymerization of the A block), and the bulk densities of the A and B components.

Helfand et al evaluated their free energy expression for the set of S, C. and L morphologies mentioned above and obtained a phase diagram denoting the stabilities of the ordered morphologies relative to the disordered phase. They also determined the scaling law for the dependence of the interdomain spacing D on N, finding $D \approx N^{0.643}$ for all three morphologies in this regime.

Noolandi et al [29, 30, 31] have presented a functional integral theory for copolymer/solvent blends and copolymer/homopolymer mixtures. This self-consistent theory makes no a-priori assumptions of weak or strong segregation limits.

Leibler [32] has developed a Landau type mean-field theory on the ODT in block copolymers and has presented the phase diagram for the microdomain morphologies in the weak segregation limits as a function of the polymer composition f and the reduced parameter χN_T, where χ represents the Flory-Huggins segment-segment interaction parameter and N_T is the total degree polymerization.

His mean-field free energy formulation consists of a fourth-order Landau expansion about its value in the disordered phase [33] in terms of vertex functions containing a suitably defined order parameter. The order parameter $\psi(\mathbf{r})$ is defined as the deviation in the local composition of one component from the spatially averaged composition. The vertex functions, describing the density-density correlations within the melt, contain the physical parameters describing the state of the system, χN_t and f.

Leibler evaluates his free energy expression for the L, C and S mesophases, developing a phase diagram valid in the weak segregation regime, very close to the critical point. He finds that the transitions form the homogeneous (disordered) phase to spheres, spheres to cylinders, and cylinders to lamellae are first order when $f \neq 0.5$. A second order transition from the disordered phase to lamellae is predicted at the critical point for the case of symmetric diblocks ($f = 0.5, \chi N_t = 10.495$). The calculation of the vertex functions is performed within a generalized random-phase approximation (RPA) [34]. Leibler uses a single harmonic to describe the sinusoidal segment density profile. This harmonic, having characteristic wave vector $\mathbf{k}^*$, is assumed to be temperature independent and characterizes the maximum in the structure factor $S(\mathbf{k}^*)$. Given these assumptions, $D \approx N^{0.5}$ in this regime.

Fredrickson and Helfand [18] have corrected Leibler's mean-field theory to take into account the effect of composition fluctuations on the ODT. Using a Hartree-type analysis, they reduce Leibler's free energy into a Brazovskii [35] form, thereby adding self-consistent corrections to the Leibler's mean-field free energy.

They observe that the ODT is weakly first order at $f = 0.5$, exhibiting a characteristic molecular weight dependence: $\chi N = 10.495 + 41.022 N^{-\frac{1}{3}}$. They also find compositional 'windows' in their phase diagram, which allows the transitions from the disordered phase to any of the ordered morphologies. Leibler's predictions are recovered when $N \to \infty$, where mean-field behavior is expected since composition fluctuations will be suppressed in this limit.

Recently, Mayes and Olvera de la Cruz [36] reevaluated Fredrickson and Helfand's free energy with consideration of the angle-dependent higher order vertex functions in their Hartree approximation and found $\chi N = 10.495 + 39.053 N^{-\frac{1}{3}}$ at $f = 0.5$. They also evaluated the free energy of Leibler using four composition harmonics instead of only one [37]. They employed nonlocal higher order vertex functions and found, upon minimization of their free energy that $\mathbf{k}^*$ is temperature dependent. Their calculations for the L and C morphologies predict a curious result $D \approx N$ in the weak segregation regime, which is different than Leibler's prediction of $D \approx N^{0.5}$. On another publication [38] the authors extended the treatment of the ODT to triblock copolymers, concluding that coupling a symmetric diblock modifies the

ODT to $\chi N = 18$. After a doubling of N is accounted for, the required difference in χ for ordering is $\approx 15\%$. For example, if χ is inversely proportional to temperature and $T_{ODT} = 100^{o}$C, the triblock copolymer would order roughly 60 °C higher than the diblock. This difference may be somewhat dependent on fluctuation corrections that have been shown to be important near the ODT [39].

2.3 Macroscopic orientation in amorphous block copolymers

Researchers have known for more than two decades that mechanically deforming a block copolymer influences the global alignment of its microdomains. Macroscopic orientation is achievable by flow, with shear alignment of the grain morphology to produce a quasi- 'single crystal' structure. In the case of lamellar diblock copolymers, the lamellar planes are typically observed within the plane of the sample [40, 41, 42, 43]. In addition to producing lamellae in the sample plane, researchers have recently observed lamellae perpendicular to the sample plane, in amorphous block copolymers, such that the normal of the lamellae is parallel to the neutral direction of the shear field [11]. Results on the macroscopic orientation of semicrystalline block copolymers will be presented in this thesis.

2.4 Semicrystalline block copolymers

Thermodynamic equilibrium is rarely achieved with polymeric materials due to the time scales associated. Is is necessary to consider other kinetic material parameters, which combine with the thermodynamically driven phase separation to define the final material morphology. For wholly amorphous block copolymers it is known that variations in processing history(temperature, mechanical stress or strain, solvents) can lead to significant alterations in the observed morphology of the bulk material [44], even though a specific equilibrium morphology is expected from thermodynamic arguments.

Microdomain formation in semicrystalline block copolymers can result either from incompatibility of the two blocks or by crystallization of one or both blocks. Phase separation due to block incompatibility leads to an amorphous two-phase melt morphology which gets locked in upon cooling. This has been demonstrated from this laboratory [51] on a polystyrene / Hydrogenated polybutadiene (SE) diblock copolymer (the E crystallizable block resembles low density polyethylene). The precursor SB unhydrogenated diblock copolymer exhibited a spherical microphase-separated morphology when spin cast from toluene. For the case of the hydrogenated SE diblock, when the solution casting temperature was below the melting point of the E block, crystallization proceeded and inhibited microphase separation, thus producing a random crystallized morphology. When casting above the E block melting point crystallization occurred within the microphase separated E domains, which where formed in the melt, and a spherical morphology resulted, similar to the SB precursor.

Several theories have been proposed to describe the equilibrium morphology of lamellar semi-crystalline diblock copolymers systems. Whitmore and Noolandi [45] developed a mean-field theory for the scaling behavior of lamellar domain spacings. They modeled the amorphous blocks as flexible chains with one end fixed at the sharp amorphous - semicrystalline interface. The semicrystalline blocks were modeled as chain-folded macromolecules with one end of the chain fixed at the interface attached to a corresponding amorphous block. They performed calculations for a poly(styrene) / poly(ethylene oxide) diblock system and found $D \approx N_T N_A^{-\frac{5}{12}}$, where N_A were the number of statistical segments in the amorphous block and N_T the total number of segments. Studies on the applicability of Noolandi's scaling law to other semicrystalline block copolymer systems have been carried out in this laboratory [46] on E/EE diblocks and elsewhere [14] on E/EP diblocks. Both studies have found good agreement with theory. Results on the validity of the scaling law for the E/EP/E triblocks will be presented in this thesis.

2.5 Gas transport in polymer systems

The transport of gases through polymer systems can be understood in terms of permeation, diffusion and solution phenomena. A steady state gas flux develops upon application of a pressure drop, which is applied across a polymer membrane. The permeation process occurs in three steps: 1) Solution of the penetrant gas into the polymer membrane from the high pressure upstream interface, 2) diffusion of the penetrant gas in the polymer and 3) evaporation of the penetrant from the membrane at the low pressure downstream surface [47].

The permeability coefficient P is expressed as the product of a kinetic term D and a thermodynamic term S the diffusion and solubility coefficients, respectively.

$$P = D * S \tag{2.1}$$

In simple terms, the permeability coefficient P is the ratio of the steady state gas flux through the polymer membrane, produced for a given driving force.

The dimensions of P are:

$$P = \frac{\text{(amount of gas under stated conditions)*(film thickness)}}{\text{(film area)*(time)*(driving pressure)}}$$

A commonly reported unit of P which will be used in this thesis is the *barrer* and is defined as

$$\frac{10^{-10}(cm^3 atSTP)(cm)}{(cm^2)(s)(cmHg)}$$

Gas transport in block copolymer systems has been the topic of two Ph.D investigations in this laboratory [48, 49]. This work will present gas permeation results on semicrystalline block copolymer systems.

Chapter 3

Experimental techniques

The E/EP and E/EP/E block copolymers were synthesized by hydrogenation of 1,4-poly (butadiene) / 1,4-poly (isoprene) block copolymers. The butadiene block consists of 10% 1,2 , 35% trans 1,4 and 55% cis 1,4 PB, while the isoprene block contains 93% cis 1,4 and 7% 3,4 PI. The catalytic hydrogenation procedure [50] has been used extensively in this laboratory [51, 46]. Hydrogenated PB thus resembles low-density polyethylene (E) and hydrogenated PI is essentially perfectly alternating ethylene propylene rubber (EP). The molecular weights of each block for the E/EP and E/EP/E block copolymers are listed in Table 3.1. These values were determined from GPC measurements on the polydiene precursors (first block and diblock or triblock), from knowledge of reactor stoichiometry and conversion, and from a previous demonstration [50] that little or no degradation occurs during the hydrogenation reactions. The melting points of the crystallizable E blocks of the series of E/EP or E/EP/E copolymers, were all between 99 and 103 °C, as determined by DSC.

A channel die, the description of which is given in detail elsewhere [52] [53] [54] [55], was used to subject the polymers to plane strain compression up to compression ratios of 11. Figure 3-1 shows a sketch of the channel die and defines the three principal directions, i.e., the lateral constraint direction (CD), the free (or flow) direction (FD), and the loading direction (LD). The channel die was maintained at a selected constant temperature during the compression flow, and the load was applied continuously until the desired compression ratios were achieved. The compressed specimens

Figure 3-1: Channel die apparatus

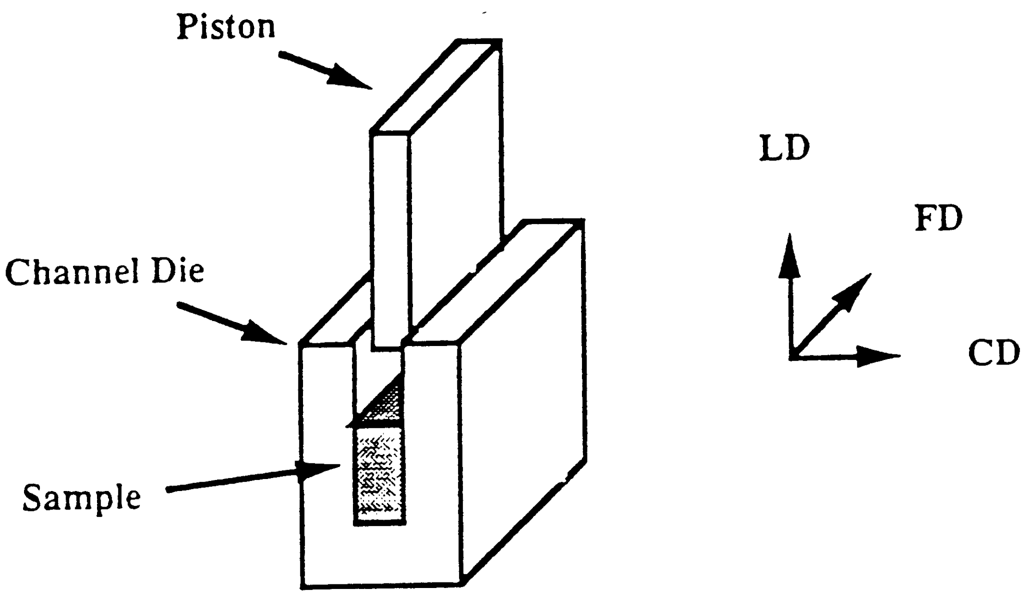

DIBLOCKS	TRIBLOCKS
E/EP 30/70	E/EP/E 15/70/15
E/EP 50/50	E/EP/E 20/60/20
E/EP 60/40	E/EP/E 25/50/25
E/EP 70/30	E/EP/E 30/40/30
E/EP 60/120	E/EP/E 35/30/35
E/EP 100/100	
E/EP 120/80	

Table 3.1: Characterization of E/EP and E/EP/E specimens
M x 10¯3 g/mole

were quenched under load to room temperature, followed by load release. The final compression ratio was determined from the reduction of the thickness of the samples.

The change in lamellar orientation due to deformation was studied by means of small-angle X-ray scattering (SAXS). The SAXS measurements were performed on a computer-controlled system consisting of a Nicolet two-dimensional position-sensitive detector associated with a Rigaku rotating-anode generator operating at 40 kV and 30 mA and providing Cu Kα radiation. The primary beam was collimated by two Ni mirrors. In this way the X-ray beam could be effectively focused onto a beam stop with a very fine size without losing much intensity. The specimen to detector distance was 2.7 m, and the scattered beam path between the specimen and the detector was enclosed by an Al tube filled with helium gas in order to minimize the background scattering. The specimen to detector distance was reduced to 10 cm when performing experiments on crystallite orientation.

A separate Rigaku wide-angle X-ray diffractometer with a rotating anode source was employed. The Cu K_α radiation generated at 50 kV and 60 mA was filtered using a thin-film Ni filter to remove the K_β signal. A Rigaku pole figure attachment was controlled on-line, and X-ray diffraction data were collected by means of a Micro VAX computer running under DMAXB Rigaku-USA software. The slit system that was used allowed for collection of the diffracted beam with a divergence angle of less than 0.3^o. Complete pole figures [54] were obtained for the projection of Euler angles of sample orientation: β from 0^o to 360^o with steps of 5^o, and α in the range 0^o to 90^o also in 5^o steps. X-ray data from the transmission and reflection modes were connected at the angle $\alpha = 50^o$. The specimen orientation was such that the flow direction FD corresponds to the Euler angles of $\alpha = 0^o \beta = 90^o$ or $\alpha = 0^o \beta = 270^o$ (rotational symmetry), the constraint direction CD was at $\alpha = 0^o \beta = 0^o$ or $\alpha = 0^o \beta = 180^o$, and the loading direction LD was at $\alpha = 90^o$ (center of the stereographic projection).

Rheological measurements were performed on a Rheometrics Dynamic Spectrometer Model RDS-II operated in the dynamics mode ($\omega = 0.1$ rad/s) with a disk - plate fixture. Dynamic shear moduli measurements were conducted using a 1% strain amplitude. The sample temperature was controlled between 70 and 150 °C using a a thermally regulated nitrogen purge. The order-disorder transition temperature was determined by measuring G' at a fixed frequency of 0.1 rad/s while slowly heating ($< 1^oC/min$) or cooling the specimens.

E/EP and E/EP/E films for permeation measurements were prepared by compression molding at 190 °C, by means of a hydraulic press. Prior to permeation measurements, the compression molded films were annealed under vacuum at 120 °C for 2 days to minimize any orientation induced by the initial molding in the press. The gases used in this study differed in size and shape: He, CO_2, CH_4, O_2, N_2. The purities of all gases were in excess of 99.99%. Gas permeability coefficients (P) were determined from steady-state measurements using a variable volume permeation apparatus [56]. All measurements were carried out at 25 °C, keeping a pressure difference of 10.5 psig across the sample films.

Chapter 4

Morphologies of E/EP and E/EP/E systems

4.1 Spherulitic E/EP and E/EP/E systems

Figure 4-1 shows the DSC curve for the E/EP 30/70 polymer. The peak centered at 100.4 °C defines the nominal melting point of polyethylene in this sample. The large breadth of the melting curve indicates the presence of a wide distribution of crystal sizes and perfection. Crystallization occurs almost instantaneously as the polymers are cooled below their melting point; varying the thermal history has little observable effect on the degree of crystallinity. Using polarized light microscopy we observed that all diblocks exhibit spherulitic morphology when crystallized from the melt, even in the samples containing as little as 30% polyethylene. These observations suggest that a lamellar morphology predominates over the entire composition range examined here. A representative micrograph of the spherulitic morphology of the E/EP and E/EP/E polymers is shown in Figure 4-2. More optical micrographs covering the entire composition range can be found in Appendix A.

Figure 4-3 shows a two-dimensional x-ray diffraction pattern, and the corresponding radial average plot of intensity (I(Q)) versus scattering vector magnitude (Q) for a typical misoriented sample used in the permeation experiments ($Q = \frac{4\pi}{\lambda} sin\theta$ and the scattering angle is 2θ). The pattern has the shape of concentric rings, with the

Figure 4-1: DSC scan for E/EP 30/70

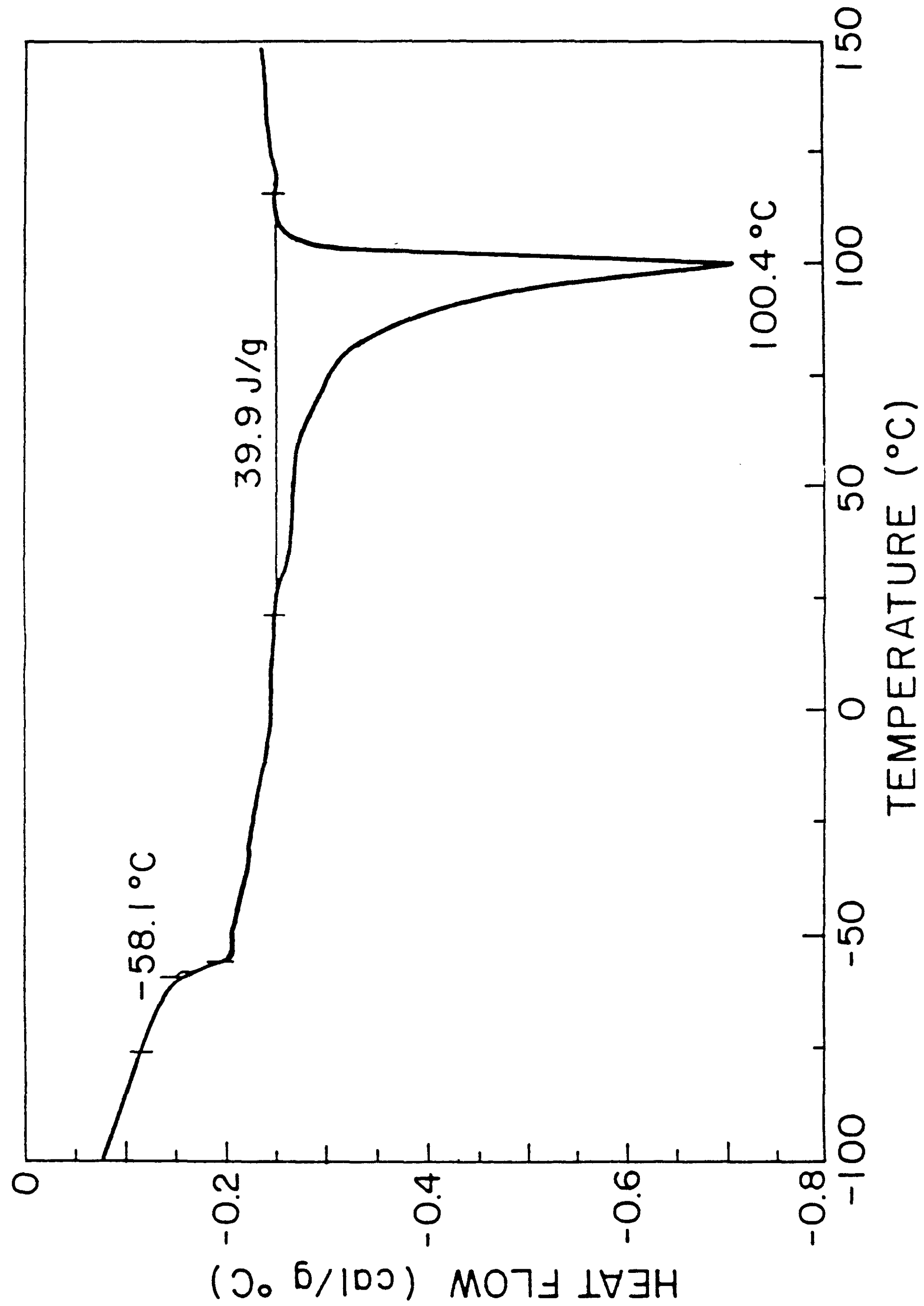

Figure 4-2: Optical micrograph E/EP 60/40 crystallized from the melt

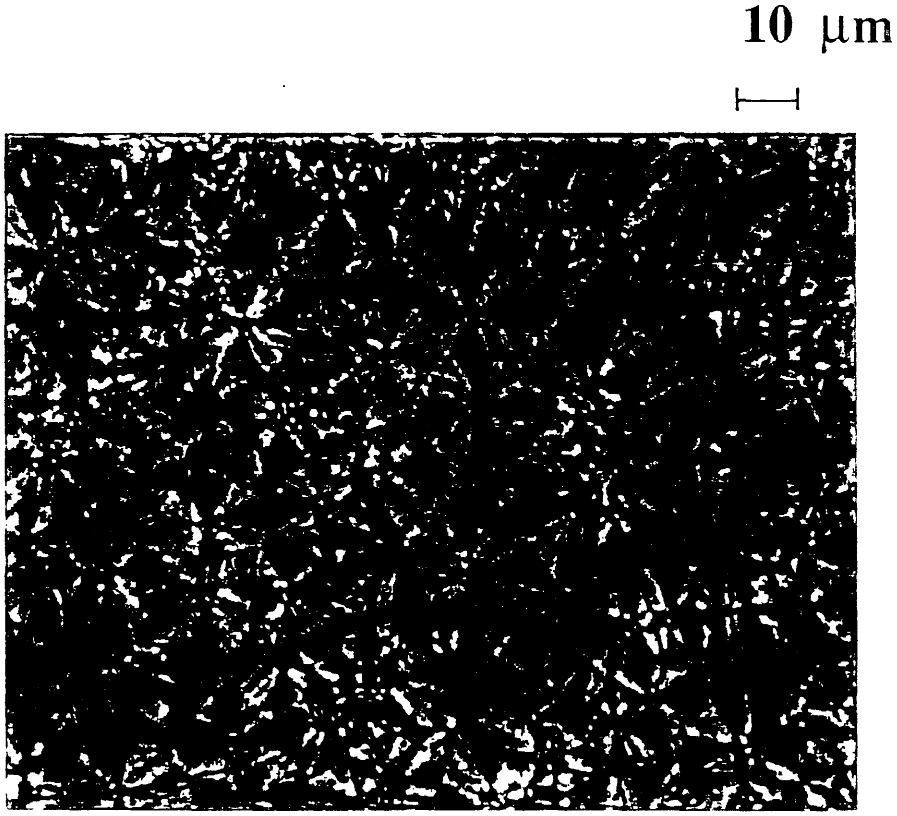

Figure 4-3: 2-D WAXS and corresponding radial average for E/EP 50/50

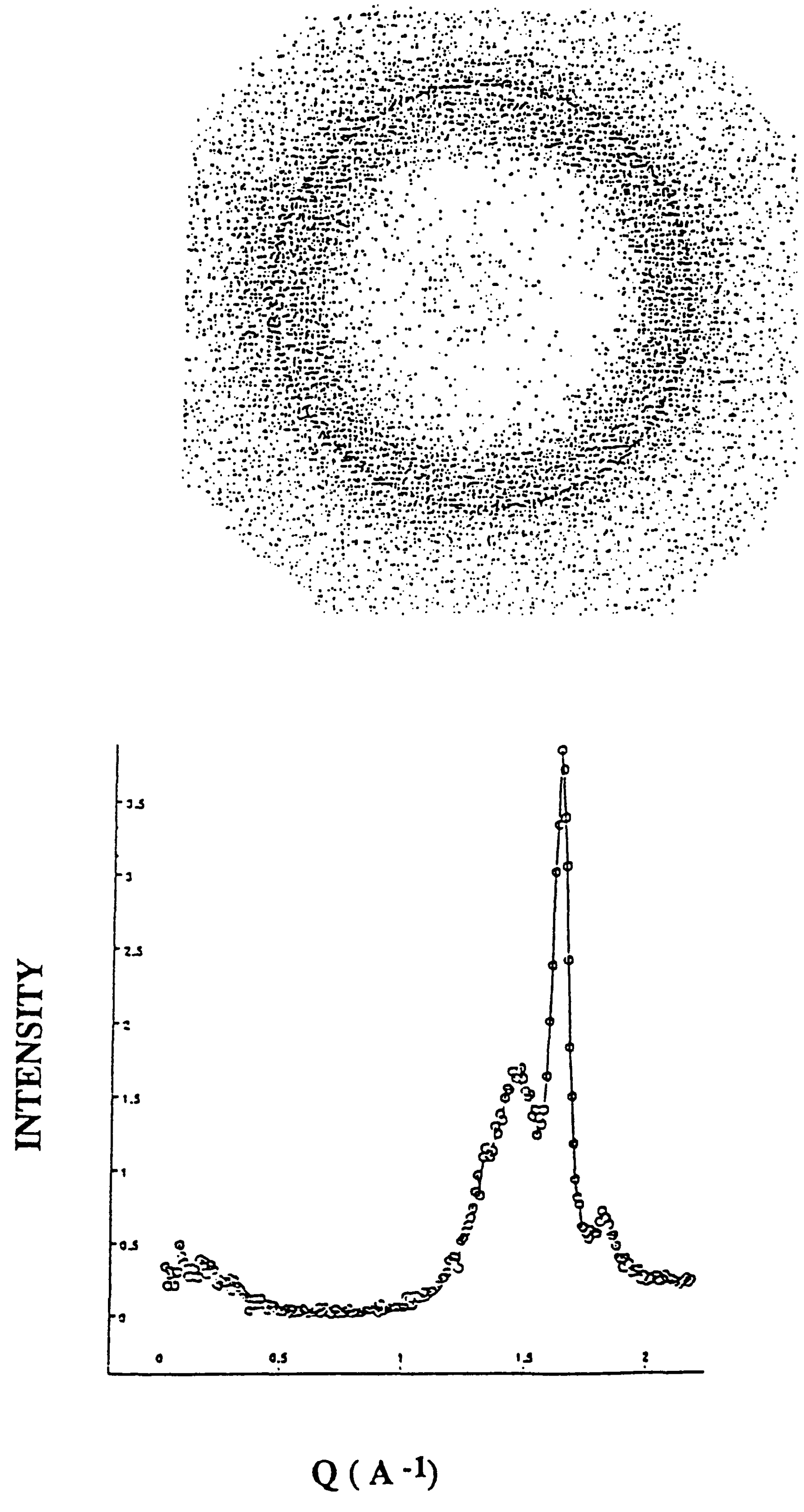

intensity being uniform along all azimuthal angles, as expected from an undeformed spherulitic specimen. The crystalline structure of undeformed spherulitic E/EP and E/EP/E polymers is observed with better resolution in Figure 4-4 in the form of 2θ scans from the wide angle diffractometer. The diffraction peaks observed in the E/EP diblock copolymers correspond to the (110), (200) and (020) diffraction planes of the orthorhombic unit cell of polyethylene [57]. In addition to the diffraction planes, a broad amorphous halo centered around $2\theta = 20^o$ is observed. The intensity of the amorphous halo increases as the amorphous block content in the diblock increases.

sample	$M\ X\ 10^{-3}\ g/mole$		$Unit\ Cell\ A^o$	
	E	EP	a	b
E/EP 30/70	30	70	7.56	4.98
E/EP 50/50	50	50	7.53	4.98
E/EP 60/40	60	40	7.52	4.96
E/EP 70/30	70	30	7.54	4.98
HDPE			7.43	4.95
E/EP 60/120	60	120		
E/EP 100/100	100	100		
E/EP 120/80	120	80		

Table 4.1: E/EP unit cell dimensions

From the positions of the peaks in the 2θ scans of the E/EP samples (Figure 4-4) it is possible to calculate the a- and b- axis dimensions of the orthorhombic unit cell using the relationship [57]

$$\frac{1}{d_{hkl^2}} = \frac{h^2}{a^2} + \frac{k^2}{b^2} + \frac{l^2}{c^2} \tag{4.1}$$

where d_{hkl} is the spacing between crystallographic planes with miller indices h, k and l, and a, b, c are the dimensions of the unit cell. The values obtained are presented in Table 4.1. It is clear that the unit cell of E/EP is slightly larger than that of the HDPE homopolymer, which is in agreement to a previous investigation in this laboratory [7] on the unit cell dimensions in semicrystalline block copolymers containing an ethylene crystallizable block, and that there is no significant trend with amorphous content or

Figure 4-4: WAXS 2-θ scans, E/EP diblocks

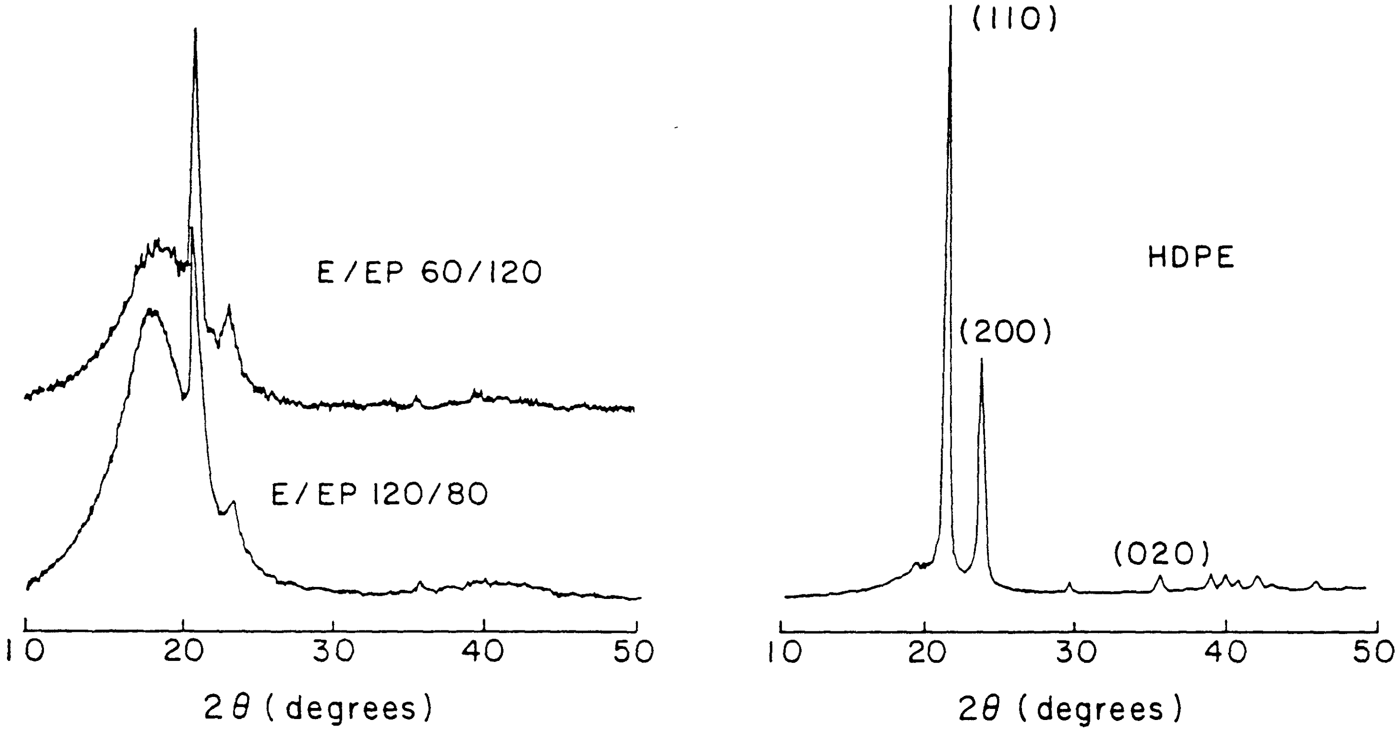

copolymer molecular weight.

4.2 E/EP channel die compression

The 2-D SAXS patterns of a representative E/EP specimen subjected to plane strain compression at 150 °C and then quenched to room temperature, are shown in Figure 4-5. The channel die experiments were conducted at compression ratios of $\lambda = 4$ to $\lambda = 12$ with no observed change in the SAXS pattern. There is no significant scattering when the x-ray beam is parallel to the constraint direction; spread-out spots on the 2D detector are observed when the sample is irradiated in the flow direction, in contrast to the sharp dots obtained when the x-ray beam is along the loading direction. The shape of the FD SAXS pattern is characteristic of the superposition pattern of lamellar stacks having different amounts of shear [58]. Figure 4-6 shows pole figures of the spatial density of normals to the (200), (020), and (110) planes for the same E/EP 50/50 specimen, which was compressed at 150 °C, i.e. well above the melting point of the E block. The pole figures represent views from the loading direction, and are shown in the form of shade plots. A linear grayscale colormap is used to represent intensity contours ranging from 5% to 90% of total intensity, with darker regions representing higher intensities of plane normals. The (200) and (020) poles are concentrated along the constraint and the flow direction respectively, indicating that the chains are oriented in the loading direction.

All diblocks of total molecular weight 100,000 g/mole exhibited the same lamellar and chain orientation when textured at 150 °C except for the E/EP 70/30 specimen. The intensity of the scattering in the 2-D SAXS pattern for this diblock was much lower than the other 100 K specimens, indicating substantially weaker lamellar orientation, and the pole figure analysis revealed no information on the chain orientation, since no clustering of poles in any particular direction was observed. The E/EP diblocks having a large total molecular weight, namely the E/EP 60/120, 120/80, and 100/100 samples showed no SAXS pattern, when deformed under the same conditions described above; this result arises because the lamellar long periods expected

Figure 4-5: SAXS of E/EP 50/50 oriented above T_m via plane strain compression: (a) x-ray beam in the loading direction, (b) x-ray beam in the flow direction

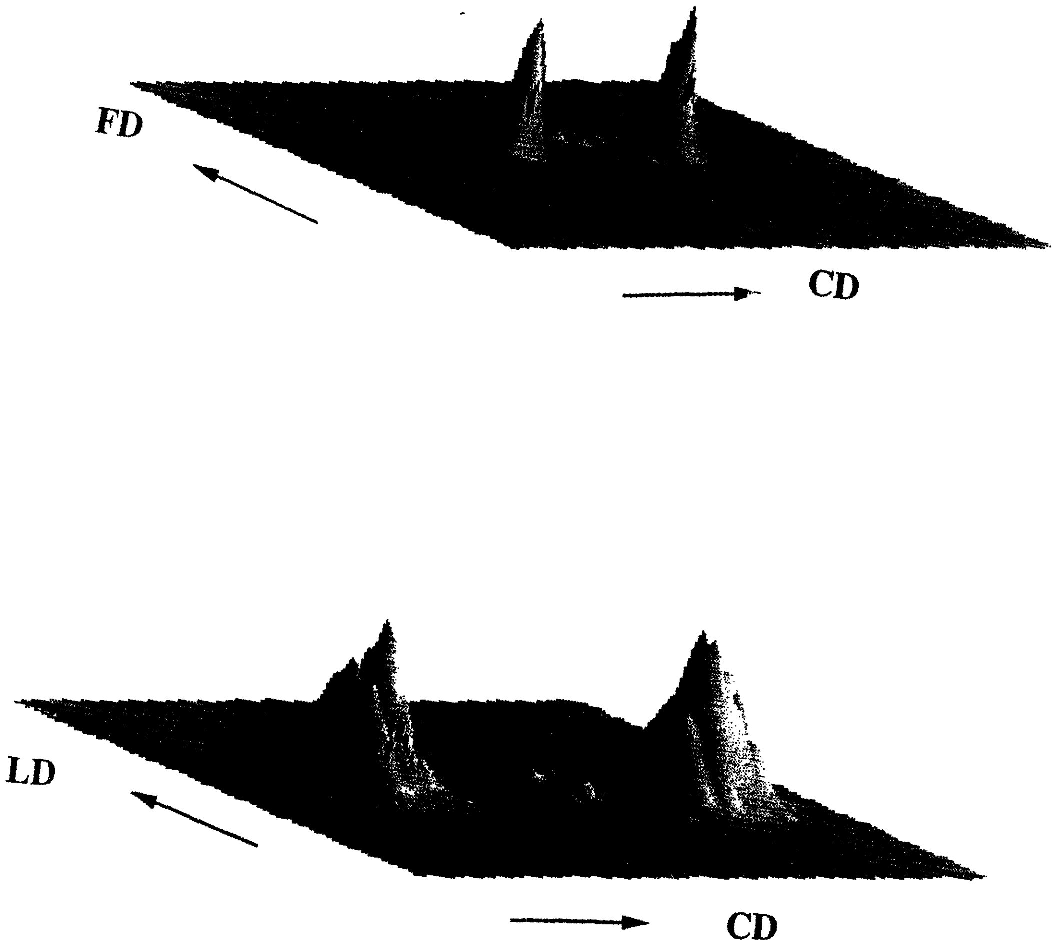

Figure 4-6: Pole figures of E/EP 50/50 oriented above T_m via plane strain compression: (a) (200), (b) (020), (c) (110) planes

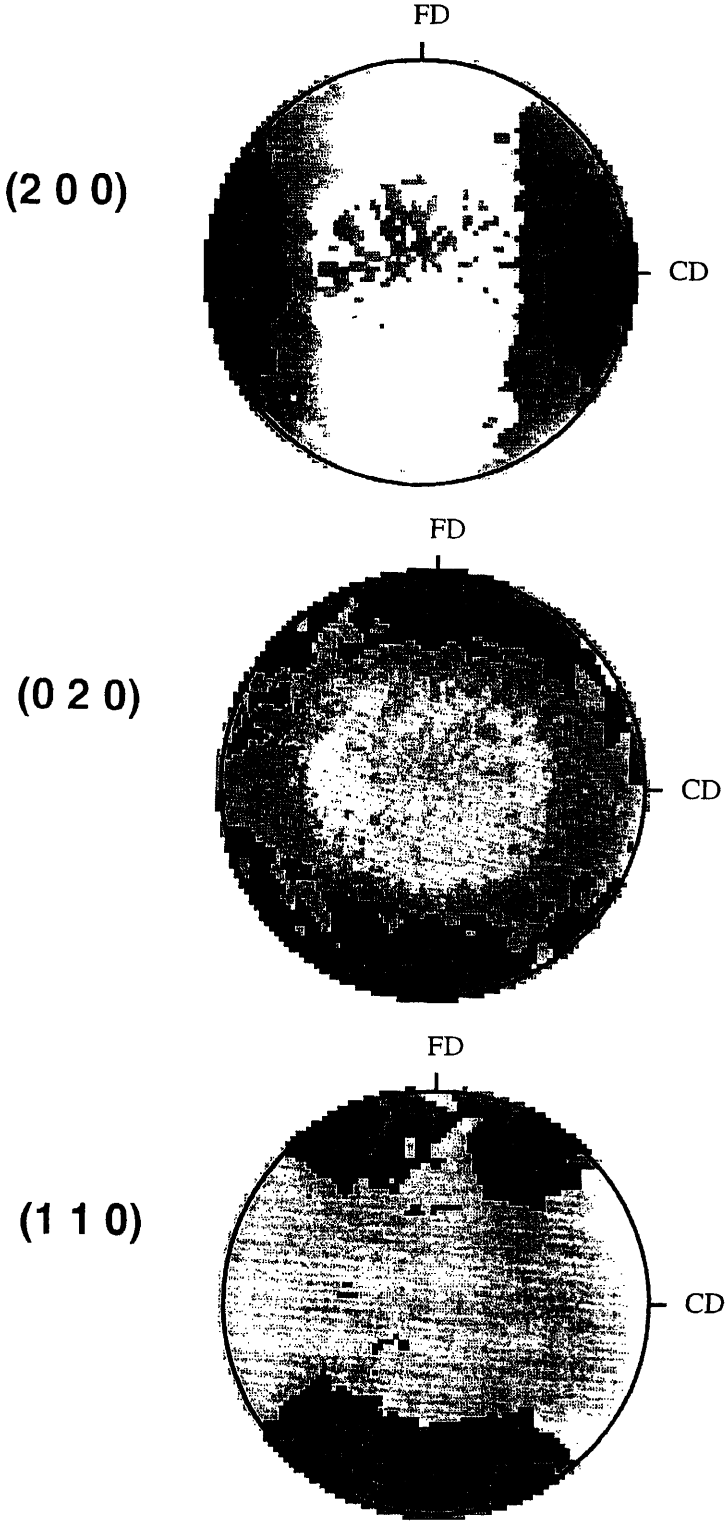

for these materials are beyond the range of detection in our SAXS equipment.

The E/EP 50/50 sample when textured at 80 °C (Figure 4-7). shows a set of SAXS patterns which are completely different from the results (Figure 4-5) obtained from the 150 °C channel die compression. The view from the loading direction reveals no scattering, arcs are observed along the loading direction upon irradiation parallel to the constraint direction, (Figure 4-7a) and broad spots are obtained when the x-ray beam is parallel to the flow direction (Figure 4-7b). The SAXS patterns thus reveal that the morphology changes from lamellae oriented perpendicular to the plane of shear when the specimen is deformed above the E block melting point, to lamellae oriented parallel to the shear plane for samples textured below the melt. The pole figures for the E/EP 50/50 specimen textured below the E block melting point (Figure 4-8), have the (200) poles in the loading direction and the (020) poles in the constraint direction, which implies that the c-axis of the polyethylene unit cell is oriented in the flow direction. Plane strain compression below the E melting point thus also results in a crystallized E chain orientation which is parallel to the plane of the lamellar superstructure.

The angle between the poles of two planes $(h_1k_1l_1)$ and $(h_2k_2l_2)$ for an orthorombic unit cell is

$$\cos\phi = \frac{\frac{h_1h_2}{a^2} + \frac{k_1k_2}{b^2} + \frac{l_1l_2}{c^2}}{\sqrt{(\frac{h_1^2}{a^2} + \frac{k_1^2}{b^2} + \frac{l_1^2}{c^2})(\frac{h_2^2}{a^2} + \frac{k_2^2}{b^2} + \frac{l_2^2}{c^2})}} \tag{4.2}$$

All the poles of the crystallographic reflections presented in Figures 4-6 and 4-8 belong to the form $< hk0 >$ and thus lie on the same plane. Using equation (2) and the values for the E/EP unit cell from Table 4.1, the location of the (110) pole lies in the CD - FD plane at an angle $\phi = 56.6^o$ with respect to (200) pole. The calculated angle ϕ between the (200) and (110) poles is in excellent agreement with the location of the (110) pole, as shown in Figure 7c, thus confirming the proposed chain orientation and the assumption of the orthorombic unit cell. For the E/EP 50/50 specimen textured at 80 °C, the same angle ϕ between the (200) and (110) poles is found in the LD-CD plane. In all of our specimens the (200) and (002) pole figures alone are sufficient to

Figure 4-7: SAXS of E/EP 50/50 oriented below T_m via plane strain compression: (a) x-ray beam in the constraint direction, (b) x-ray beam in the flow direction

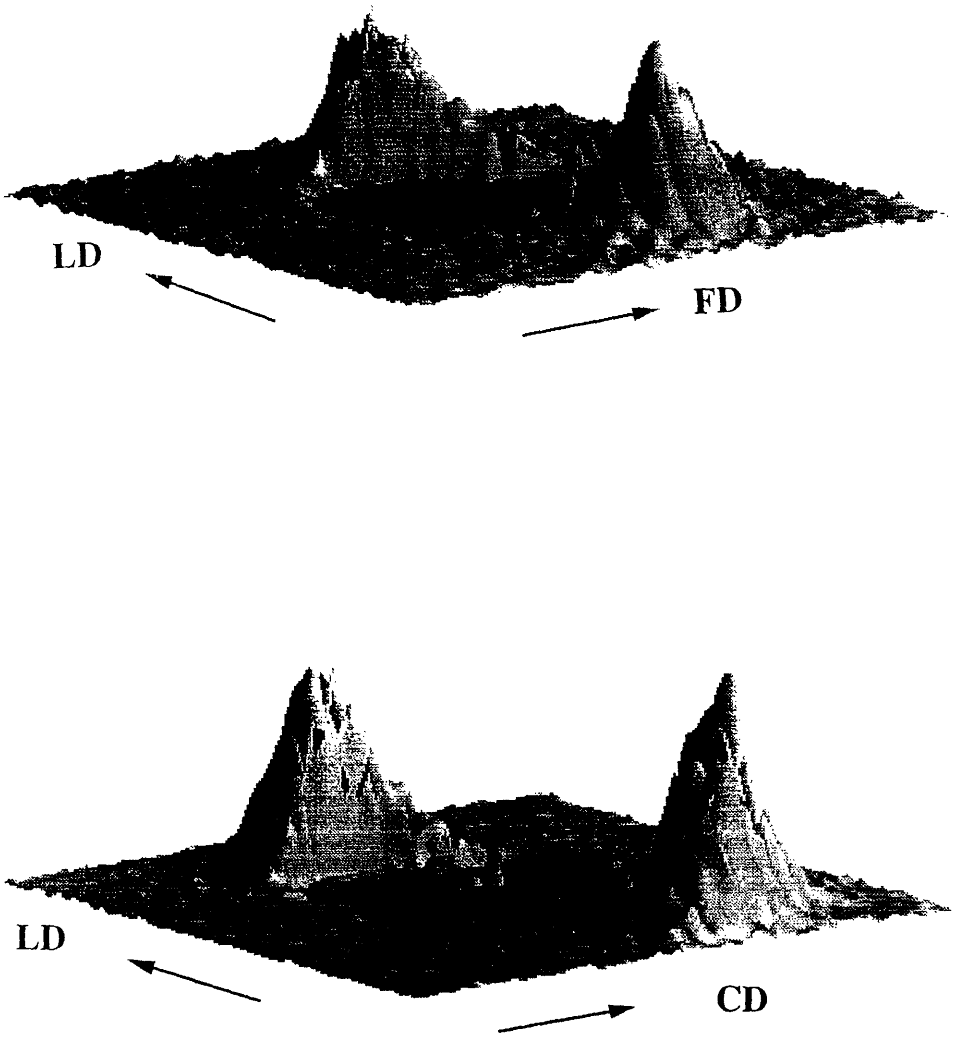

Figure 4-8: Pole figures of the E/EP 50/50 diblock oriented below T_m via plane strain compression: (a) (200), (b) (020), (c) (110) planes

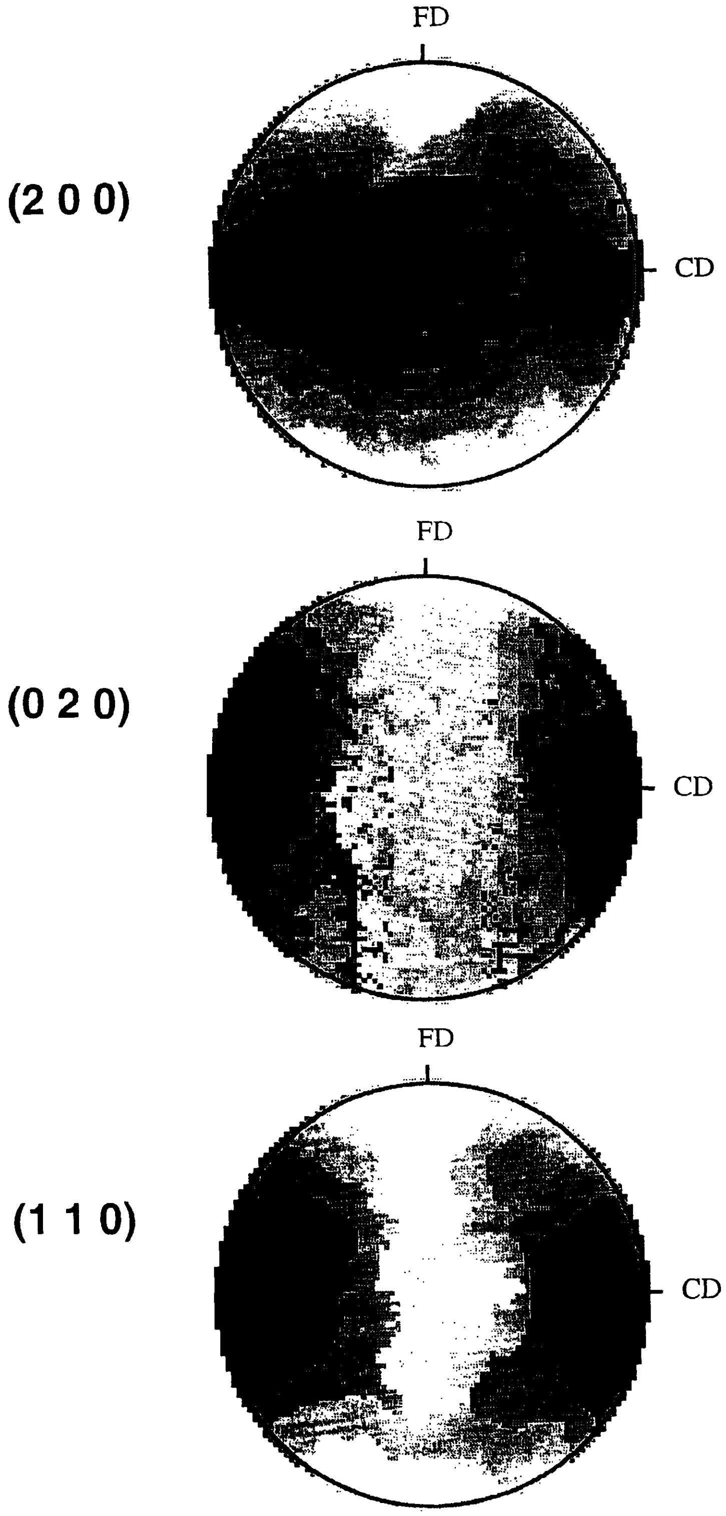

determine the unit cell orientation. The (110) pole figures are presented however, as additional supporting evidence to confirm the proposed unit cell orientations.

The average intensities of the SAXS patterns of the channel die samples at 150 °C were calculated for rectangular slices along the lamellar normal, i.e the CD direction, to determine the lamellar long periods D_{LD}, D_{FD}, and a representative plot is shown in Figure 4-9 as a plot of intensity $I(Q)$ versus scattering vector magnitude Q ($Q = \frac{4\pi}{\lambda} sin\theta$ and the scattering angle is 2θ). The averaged SAXS spectra for the other E/EP diblocks can be found in Appendix B. Because of the symmetry of the SAXS pattern there are always two peaks at $+Q$ and $-Q$. The absence of data points around $Q = 0$ is due to the beamstop. The data are shown with solid points together with a solid line representing a cubic smoothing spline fit. Table 4.2 compares the lamellar long periods D_{LD}, D_{FD} calculated for each specimen from the integrated SAXS spectra of Figure 4-9. The FD spectra show somewhat shorter average D-spacings than the ones calculated from the LD SAXS spectra, but the difference is within the 10% error range in the calculation of the lamellar long periods.

The results for the lamellar orientation and the unit cell orientation within the crystallized lamellae in the textured E/EP 100 K diblocks, as deduced from the pole figure and SAXS analysis, are summarized schematically in Figure 4-10.

sample	$D_{LD}(A^o)$	$D_{FD}(A^o)$
E/EP 30/70	618	598
E/EP 50/50	601	557
E/EP 60/40	665	604
E/EP 70/30	556	551

Table 4.2: Lamellar long periods for channel die E/EP samples at T=150 °C.

Figure 4-9: Averaged SAXS spectra for the uniaxially compressed E/EP 60/40 diblock above T_m: (LD) x-ray beam in the loading direction, (FD) x-ray beam in the flow direction

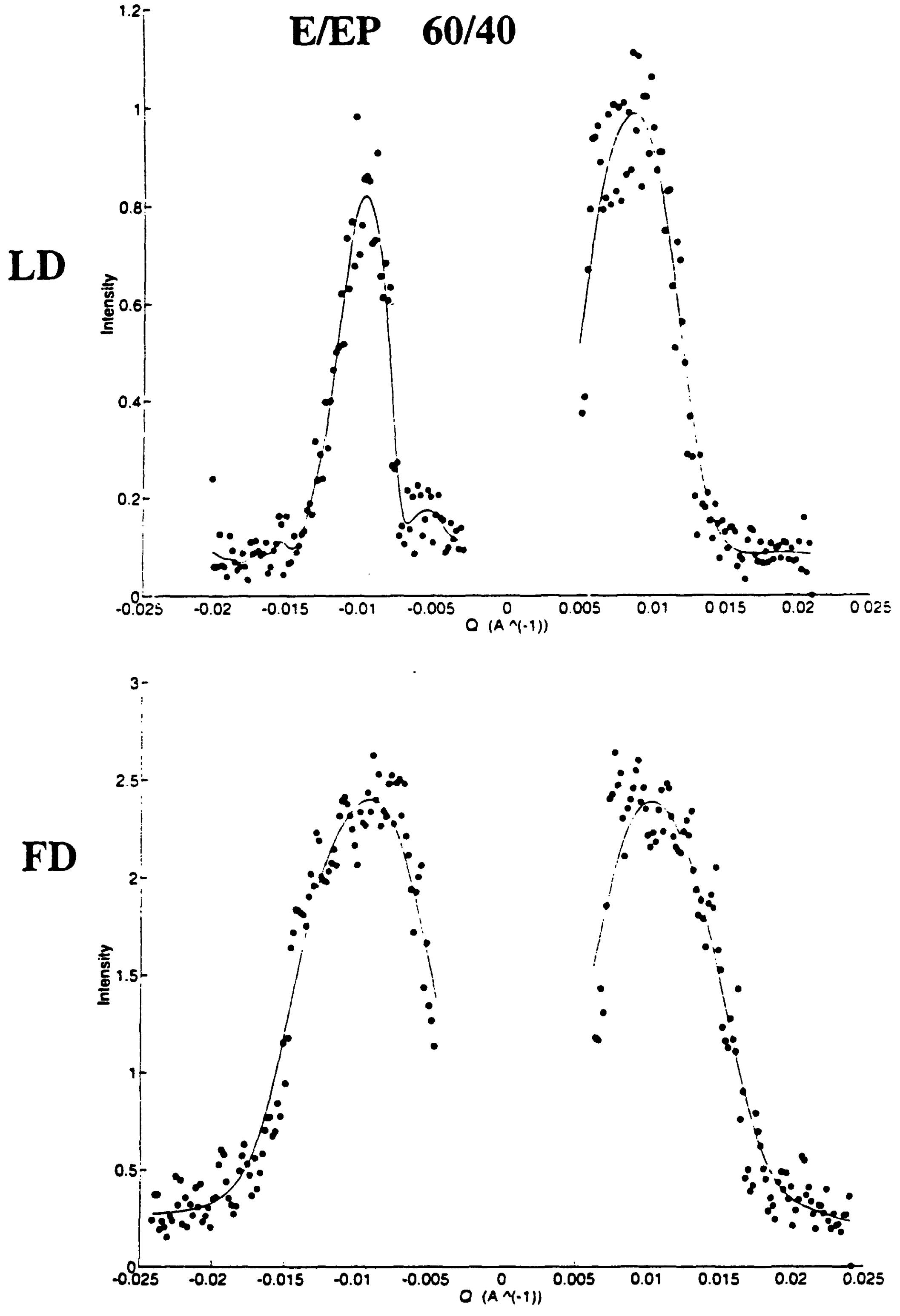

Figure 4-10: Sketch of lamellar and unit cell orientation in E/EP specimens processed above (a) and below (b) the E block melting point
Insert shows the orientation of the orthorhombic PE unit cell

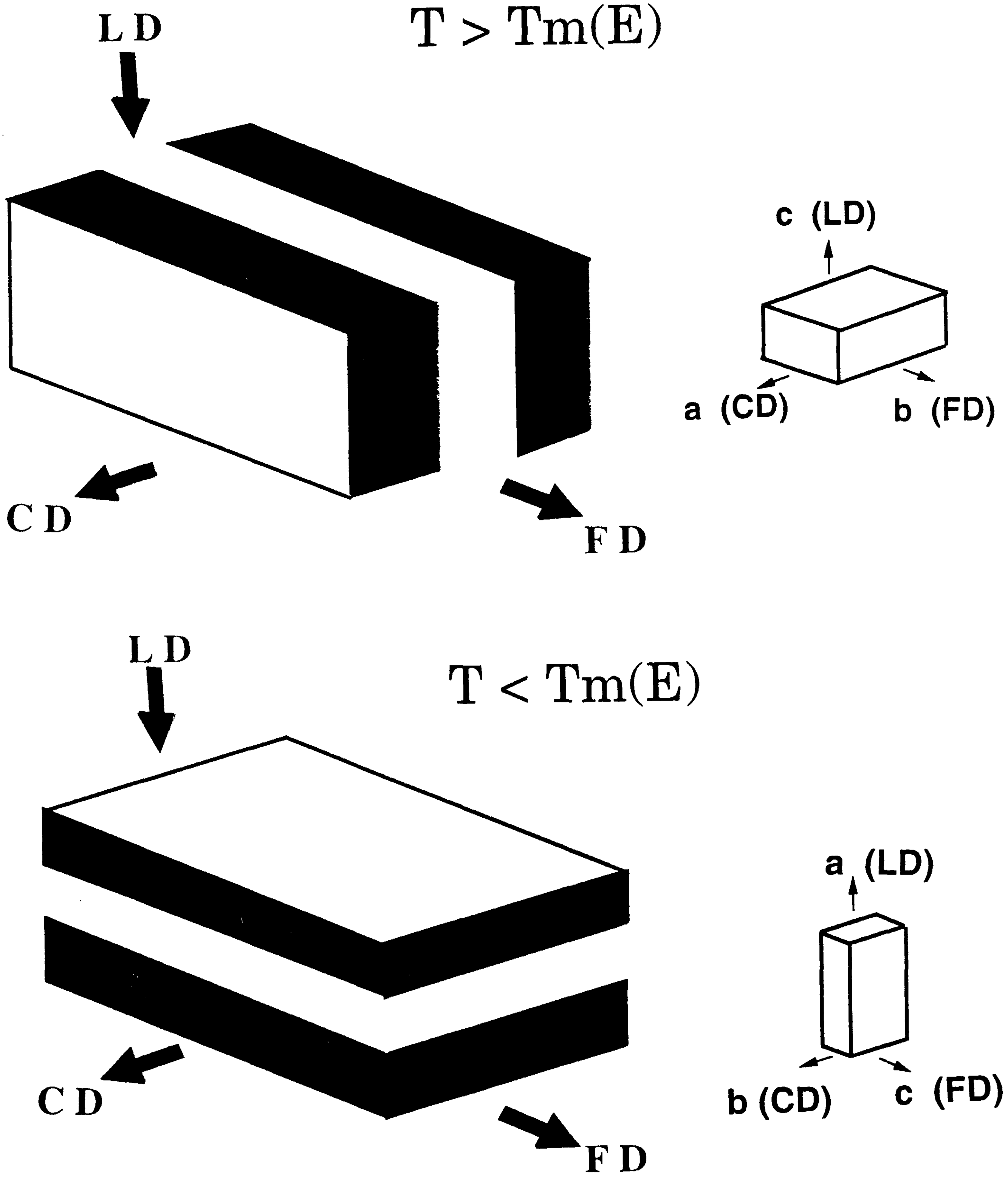

4.3 E/EP/E channel die compression and ODT determination

The 2-D SAXS patterns of the E/EP/E 25/50/25 specimen subjected to plane strain compression at 150 °C and then quenched to room temperature, are shown in Figure 4-11. The channel die experiments were conducted at compression ratios of $\lambda = 4$ to $\lambda = 12$, and an applied stress $\sigma = 8.0MPa$, with no observed change in the SAXS pattern. There is no significant scattering when the x-ray beam is parallel to the constraint direction; Spread-out spots on the 2D detector are observed when the sample is irradiated in the flow direction, in contrast to the sharp dots obtained when the x-ray beam is along the loading direction.

The E/EP 25/50/25 sample when textured at 150 °C (Figure 4-12) at an applied stress of $\sigma = 2.4MPa$ shows a set of SAXS patterns which are completely different from the results (Figure 4-11) obtained from the 150 °C channel die compression at higher applied stresses $\sigma = 8.0MPa$. The view from the loading direction reveals no scattering, arcs are observed along the loading direction upon irradiation parallel to the constraint direction, (Figure 4-12a) and broad spots are obtained when the x-ray beam is parallel to the flow direction (Figure 4-12b). The SAXS patterns thus reveal that the morphology changes from lamellae oriented perpendicular to the plane of shear when the specimen is deformed at high applied stress (8.0 MPa), to lamellae oriented parallel to the shear plane for samples textured at low applied stress (2.4 MPa).

The behavior of the E/EP/E 25/50/25 triblock in the melt was investigated by performing a SAXS temperature study, and by DSC. The DSC spectrum of the triblock is shown in Figure 4-13. The peak centered at 99 °C defines the nominal melting point of polyethylene in this sample. The large breadth of the melting curve indicates the presence of a wide distribution of crystal sizes and perfection. Channel die specimens were prepared using an applied stress of $\sigma = 8.0MPa$ at 150 °C, so that the orientation produced would be lamellae perpendicular to the plane of shear (Figure 4-14a). The samples were mounted on a Metler hotstage, which was placed

Figure 4-11: SAXS of E/EP/E 25/50/25 oriented above the E block melting point via plane strain compression: $\lambda = 4$ to $\lambda = 12, \sigma = 8.0 MPa$
(a) x-ray beam in the loading direction, (b) x-ray beam in the flow direction

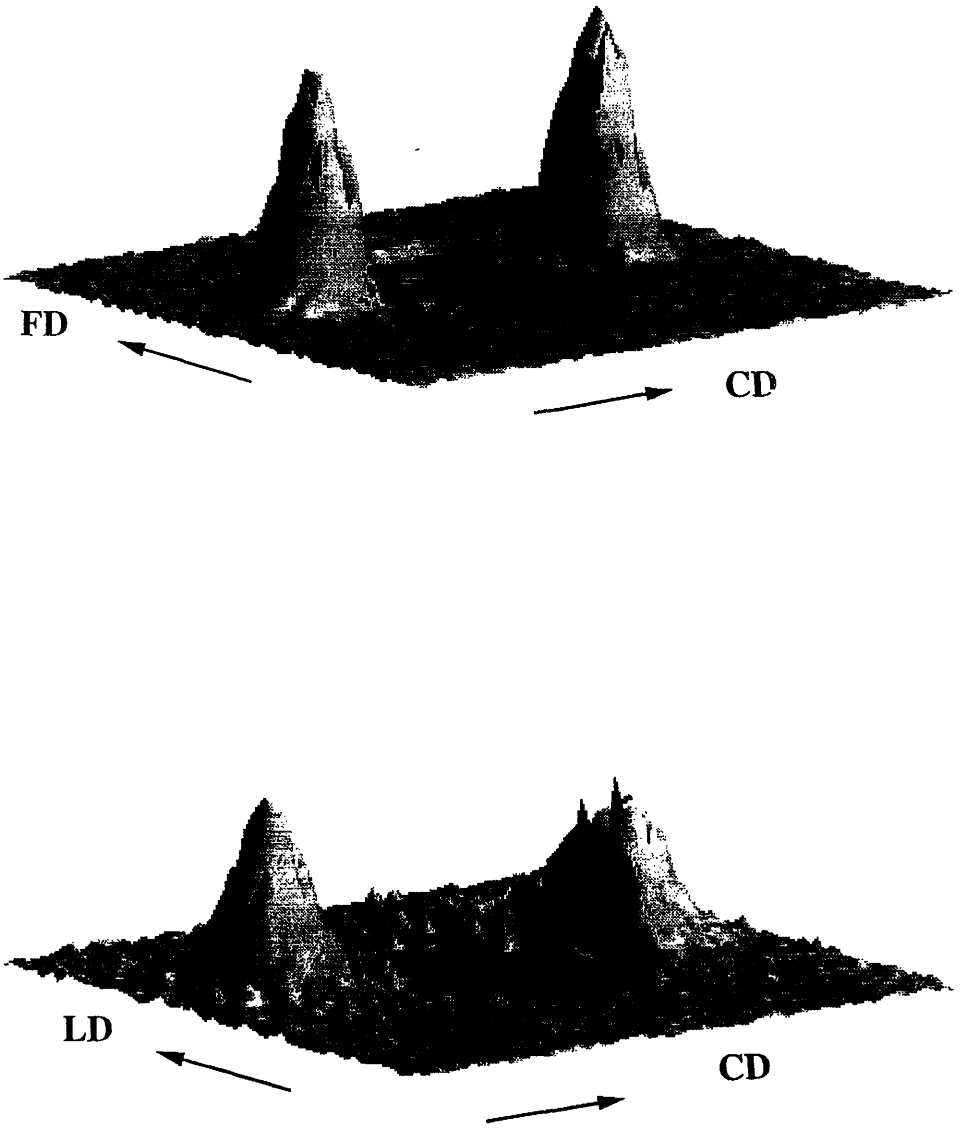

Figure 4-12: SAXS of E/EP/E 25/50/25 oriented above the E block melting point via plane strain compression: $\lambda = 4$ to $\lambda = 12, \sigma = 2.4MPa$
(a) x-ray beam in the constraint direction , (b) x-ray beam in the flow direction

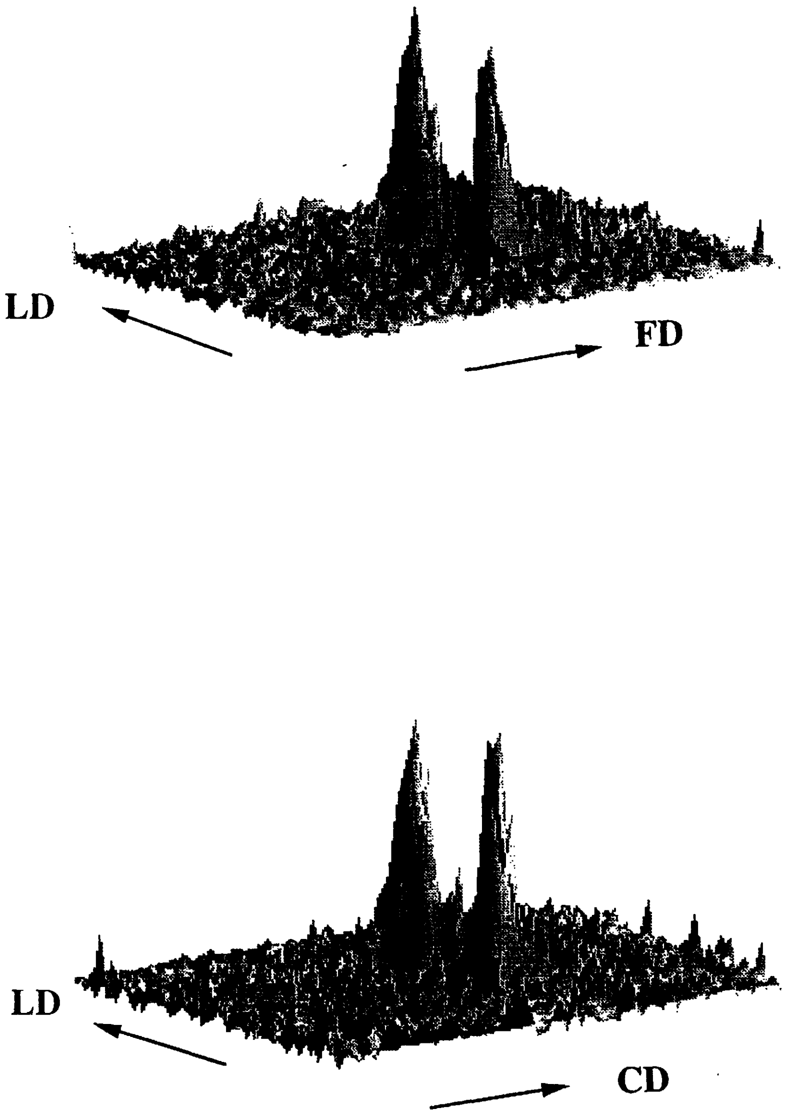

Figure 4-13: DSC scan for E/EP/E 25/50/25

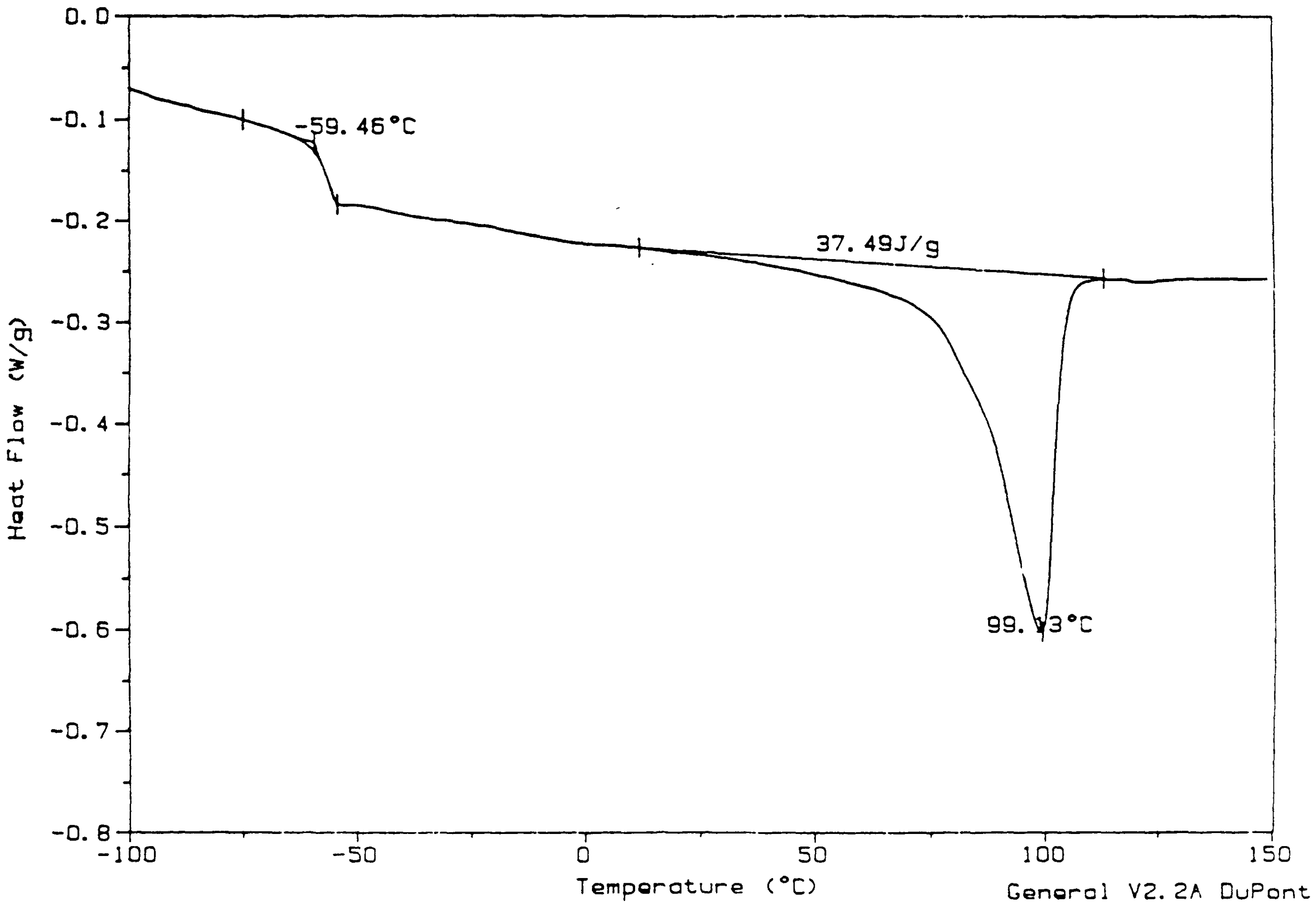

Figure 4-14: SAXS temperature study of E/EP/E 25/50/25 oriented above the E block melting point via plane strain compression, $\sigma = 8.0MPa$, x-ray beam in the loading direction
(a) 25^oC, (b) 80^oC, (c)$100^oC(melt)$ (d) Annealed for 24 hrs at 105^oC, cooled to 25^oC (e) Annealed for 24 hrs at 106^oC, cooled to 25^oC

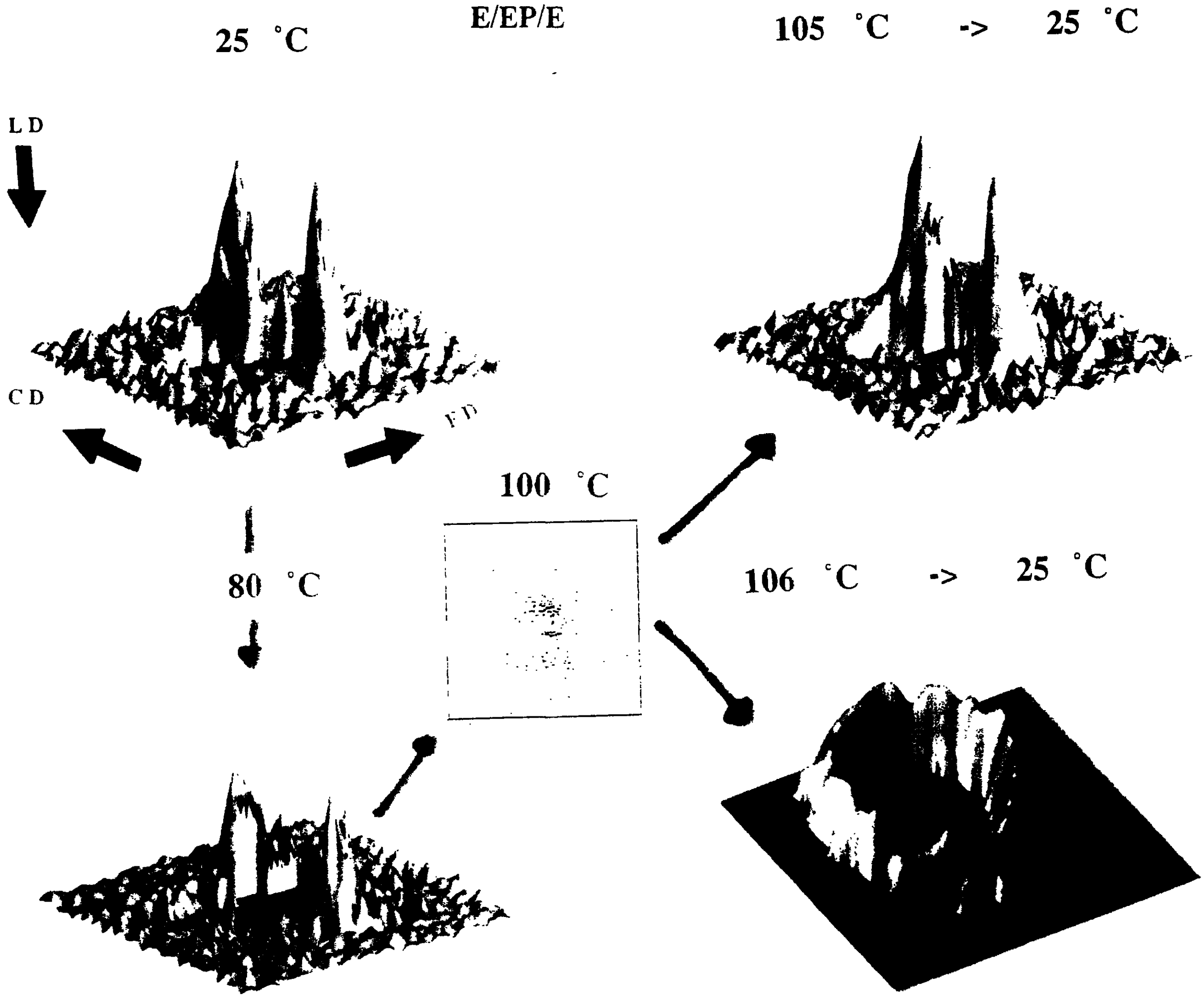

within the x-ray beam path. In that way, SAXS spectra at different temperatures could be taken in situ.

As the E/EP/E channel die triblocks are heated towards the 99^oC melting point, the LD-SAXS pattern still shows orientation in the constraint direction, but the intensity is reduced (see Figure 4-14b, $T = 80^oC$), and finally no scattering is observed at temperatures above the E block melting point (4-14c, $T = 100^oC$). The contrast in the x-ray spectrum is provided by the crystalline E phase. The crystallites in the E/EP/E triblock start melting as the 99 ^oC melting point is approached, thus reducing the observed SAXS intensity. No SAXS pattern can be observed at temperature above the melt, since there are no more crystallites to provide contrast. The absence of contrast in the melt SAXS pattern does not necessarily imply the existence of a homogeneous melt. To enquire into the possibility of the existence of a heterogeneous melt under shear, the E/EP/E samples were annealed at 105^oC (Figure 4-14d) and 106^oC (Figure 4-14e) for 24 hours and then cooled back to room temperature. Samples heated up to 105^oC and annealed for a day, recovered their original oriented perpendicular lamellar morphology when cooled back to room temperature. Crystallization occurred within an already oriented, microphase separated, melt to reproduce the original oriented morphology. Annealing at 105^oC actually *improved* the lamellar orientation, as evidenced by the increase in intensity of SAXS pattern observed after cooling back to room temperature. The room temperature ring SAXS pattern of the E/EP/E channel died sample annealed at 106^oC (Figure 4-14e) indicates that at 106^oC the melt is homogeneous and crystallization produced a random spherulitic morphology, similar to what is shown in the optical micrographs of Appendix A. Therefore, between 105 and 106 °C a transition occurred from an ordered to a disordered melt.

This order-disorder transition (ODT) was further investigated using rheological measurements. Low frequency ($\omega = 0.1 rad/s$) dynamic isochronal dynamic elastic shear moduli were obtained while heating or cooling a specimen at a rate of 1 ^oC per 5 minutes. At the weakly first order ODT the elasticity drops discontinuously, signaling the 'melting' of the ordered structure to a disordered, viscous fluid state. The results

Figure 4-15: Rheological measurements of E/EP/E 25/50/25
$\omega = 0.1$ rad/s, 1% strain amplitude
(a) Dynamic shear moduli upon heating
(d) Dynamic shear moduli upon cooling

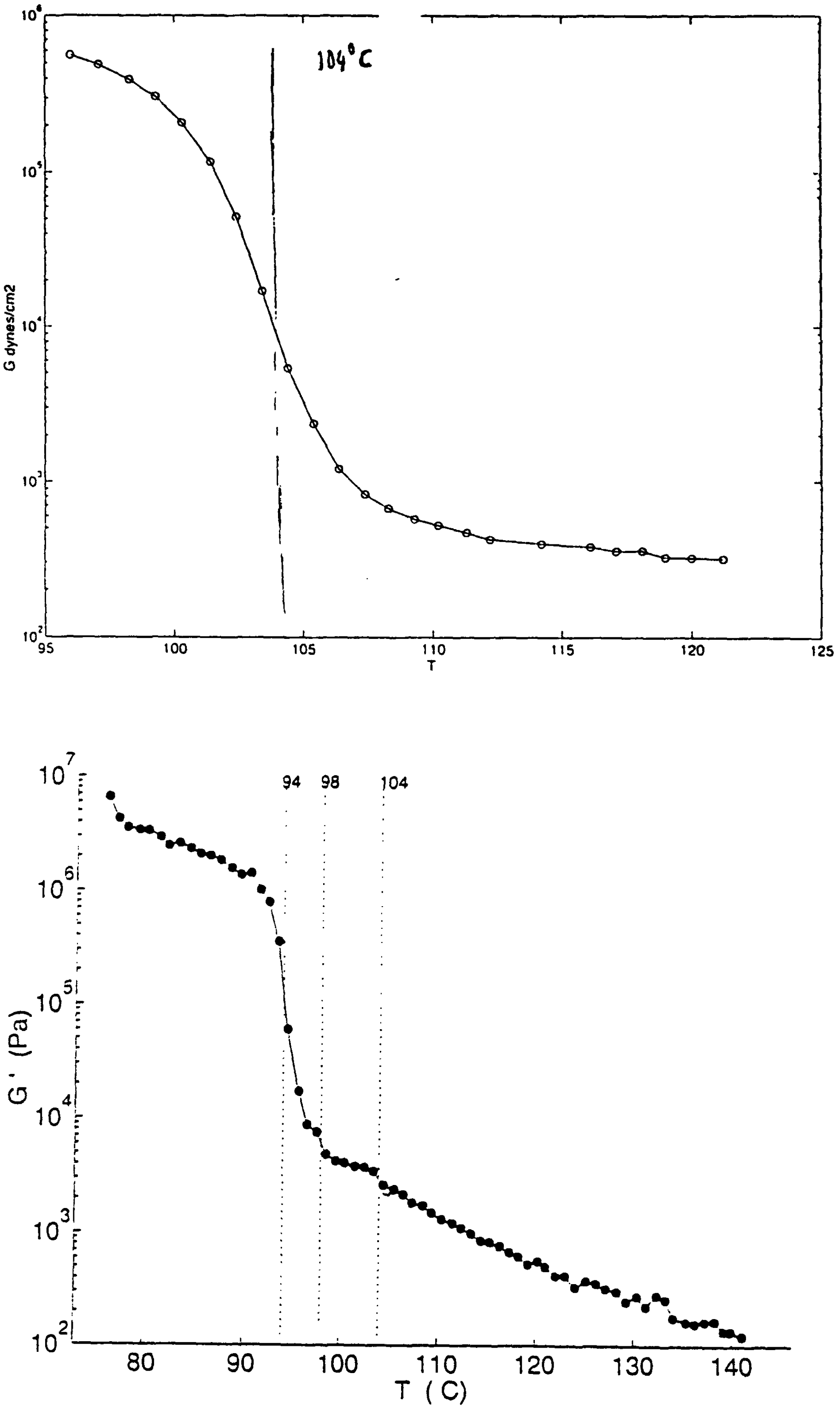

of such measurements are shown in Figure 4-15. The ODT thus determined of $T = 104^oC$ by the change in slope in the G' versus T plots is in excellent agreement with the SAXS value of 106°C.

4.4 Evaluation of the Noolandi scaling law for E/EP/E systems

The E/EP spherulitic samples showed no structure on our SAXS equipment. A SAXS pattern could only be obtained on the oriented diblocks. This arises because the lamellar long periods expected for the triblock materials are beyond the range of detection in our SAXS equipment. We were, however, able to measure the lamellar long periods for the E/EP/E triblocks and compare the scaling behavior of lamellar domain spacings D with varying amorphous block content.

The radial average intensities of the SAXS patterns for the spherulitic triblocks were calculated to determine the lamellar long periods D. The plots are shown Figure 4-16 as a plot of intensity $I(Q)$ versus scattering vector magnitude Q. The data is plotted as solid points together with a solid line representing a cubic smoothing spline fit.

Figure 4-17 is a plot of D versus amorphous content, in the form of Noolandi's scaling law (See Chapter 2.4). The theory predicts a straight line having a slope of $s_1 = -\frac{5}{12} = -0.417$. A calculated line of slope s_1 is shown for comparison with the actual experimental data. The position of the calculated (dashed) line on the vertical axis has been arbitrarily chosen to better illustrate the relationship between predicted and experimental slopes. The least squares best fit to the experimental data for the E/EP/E samples (solid line) gives a slope of $s_2 = -0.122$. It is obvious that the data does not fit perfectly the scaling law, but the general trend with increasing amorphous content is shown clearly, particularly in Figure 4-18, which shows a plot of the lamellar long periods D calculated for each specimen from the integrated SAXS spectra of Figure 4-16 versus the percentage of the EP block in the specimen. As expected, D decreases with increasing amorphous content.

Figure 4-16: Averaged SAXS spectra for E/EP/E spherulitic specimens

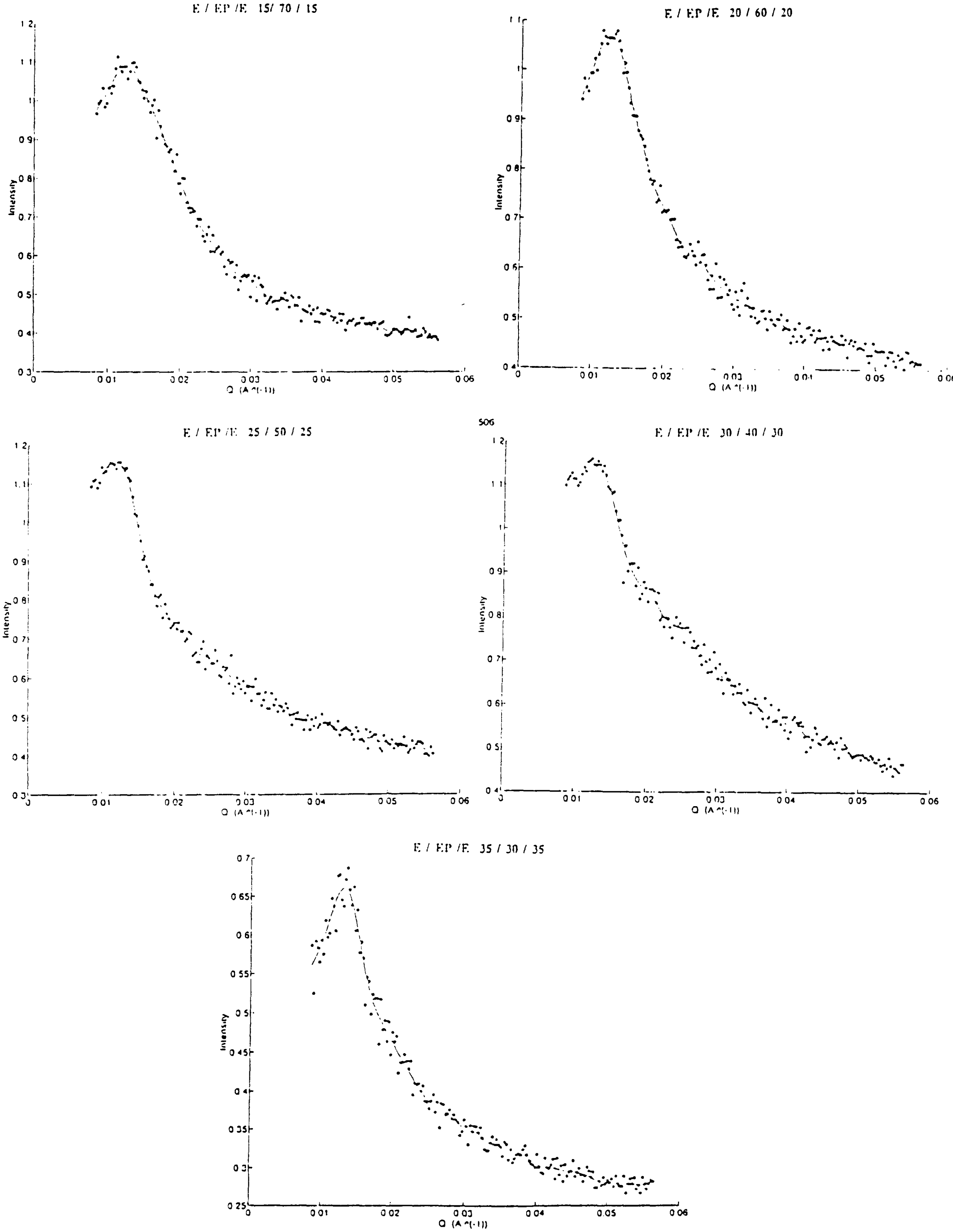

Figure 4-17: Noolandi scaling law for E/EP/E spherulitic specimens

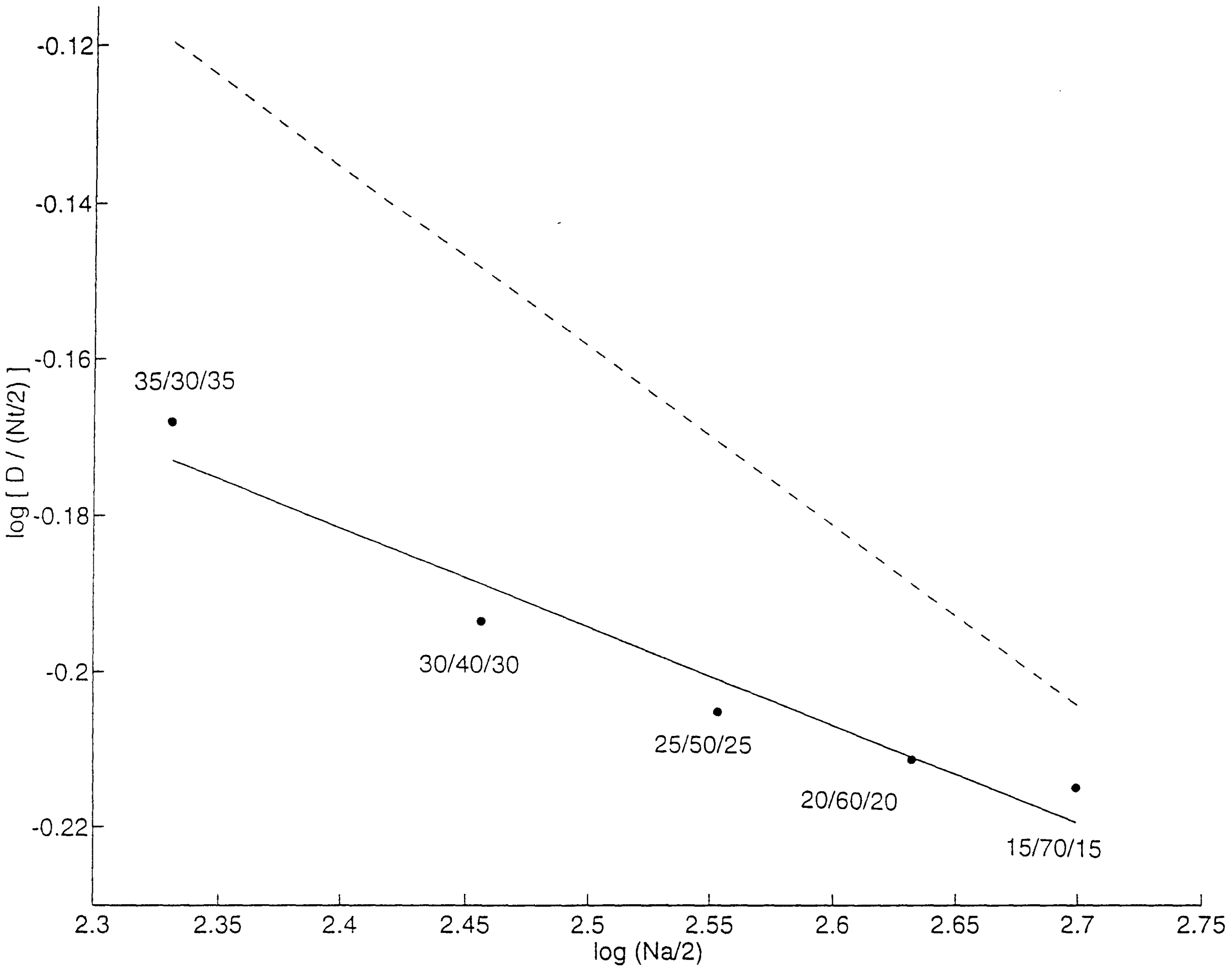

Figure 4-18: Lamellar long periods for E/EP/E spherulitic specimens

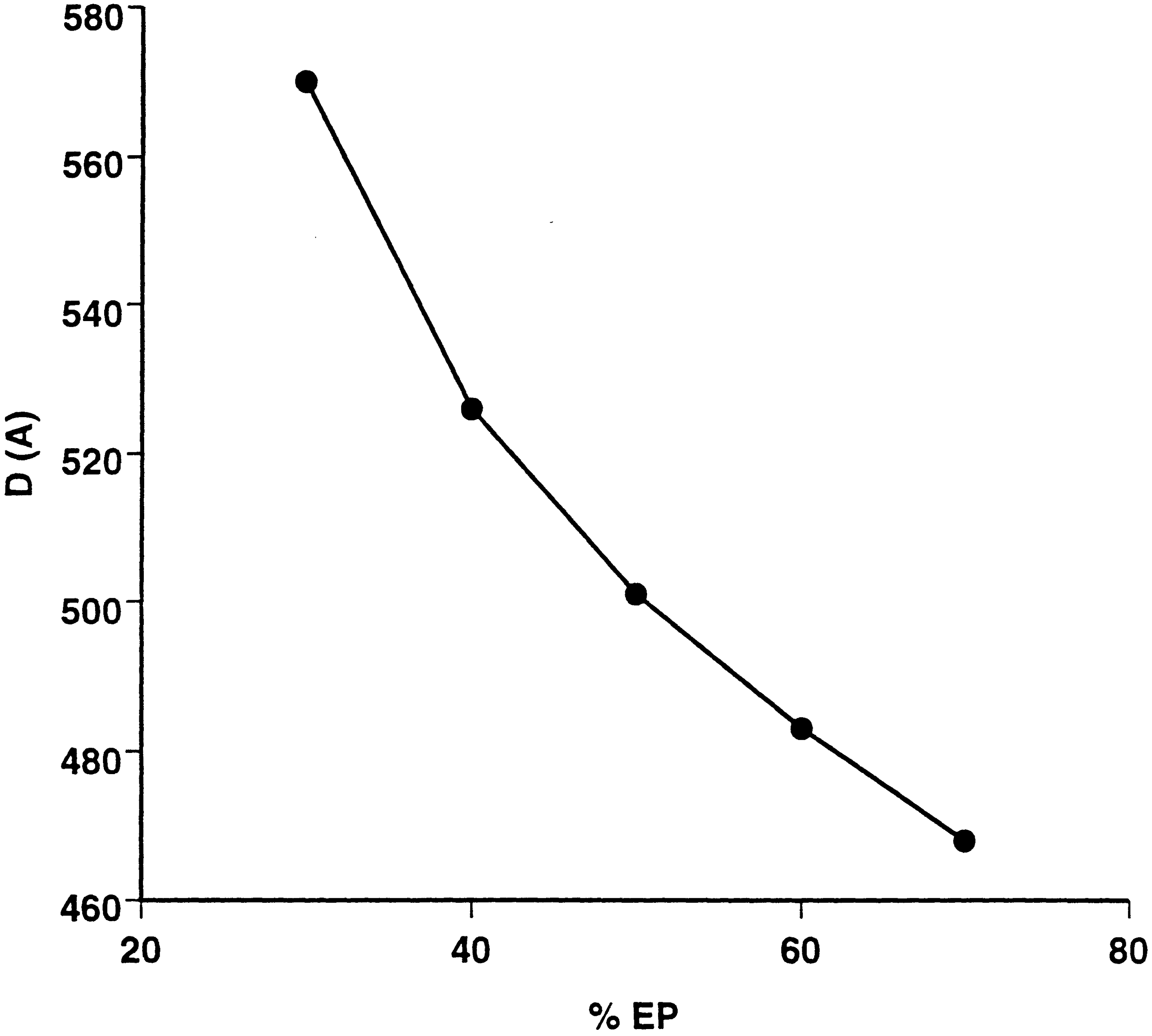

4.5 Discussion

The behavior of the E/EP and E/EP/E block copolymers when textured in the melt, can be rationalized from an examination of the position of the specimens with respect to Leibler's phase diagram [32] and using the results of previous studies on wholly amorphous diblock copolymers [11]. The block copolymers we examined contained two long sequences with N_A and N_B units of chemically distinct segments. At sufficiently high temperatures (or low total degree of polymerization $N_T = N_A + N_B$) the melt is disordered or homogeneous, while at low temperatures (or high N_T) various ordered structures [32](lamellar,OBDD, hexagonal,cubic) are observed. Equilibrium phase behavior was expressed by Leibler in terms of the polymer composition f and the reduced parameter χN_T, where χ represents the Flory-Huggins segment-segment interaction parameter. χN_T for each of our E/EP and E/EP/E copolymer systems was calculated using χ values reported by Bates et al [59]; the results are plotted versus the E fraction in the copolymer in the format of Leibler's phase diagram at 120 °C in Figure 4-19. The highest molecular weight diblocks for this study (upper row of solid points on the phase diagram) are clearly above the order-disorder boundary at the selected temperature, thus indicating that at equilibrium they form heterogeneous melts; the 100 K diblocks and the triblocks, however, are very close to the order-disorder transition (ODT).

The results shown in Figure 4-19 show that all of our 100K diblocks and triblocks are being processed in the 150 °C channel die experiments exactly in the regime near the ODT in which fluctuations [11] dominate the lamellar structure of the melt. In this regime of the morphological phase diagram, other diblock copolymers have already been shown to respond to shear deformation by organizing their lamellar structure perpendicular to the plane of shear [9]. This study examined dynamically sheared poly(ethylene - propylene) / poly (ethylethylene) (EP/EE) diblock copolymer melts sheared near T_{ODT}, which exhibited the parallel lamellar orientation at low shear frequencies and the perpendicular orientation at higher frequencies. At temperatures further away from the ODT, the parallel orientation was obtained at all frequencies.

Figure 4-19: Position of the E/EP and E/EP/E copolymers relative to the order-disorder transition curve of Leibler's phase diagram

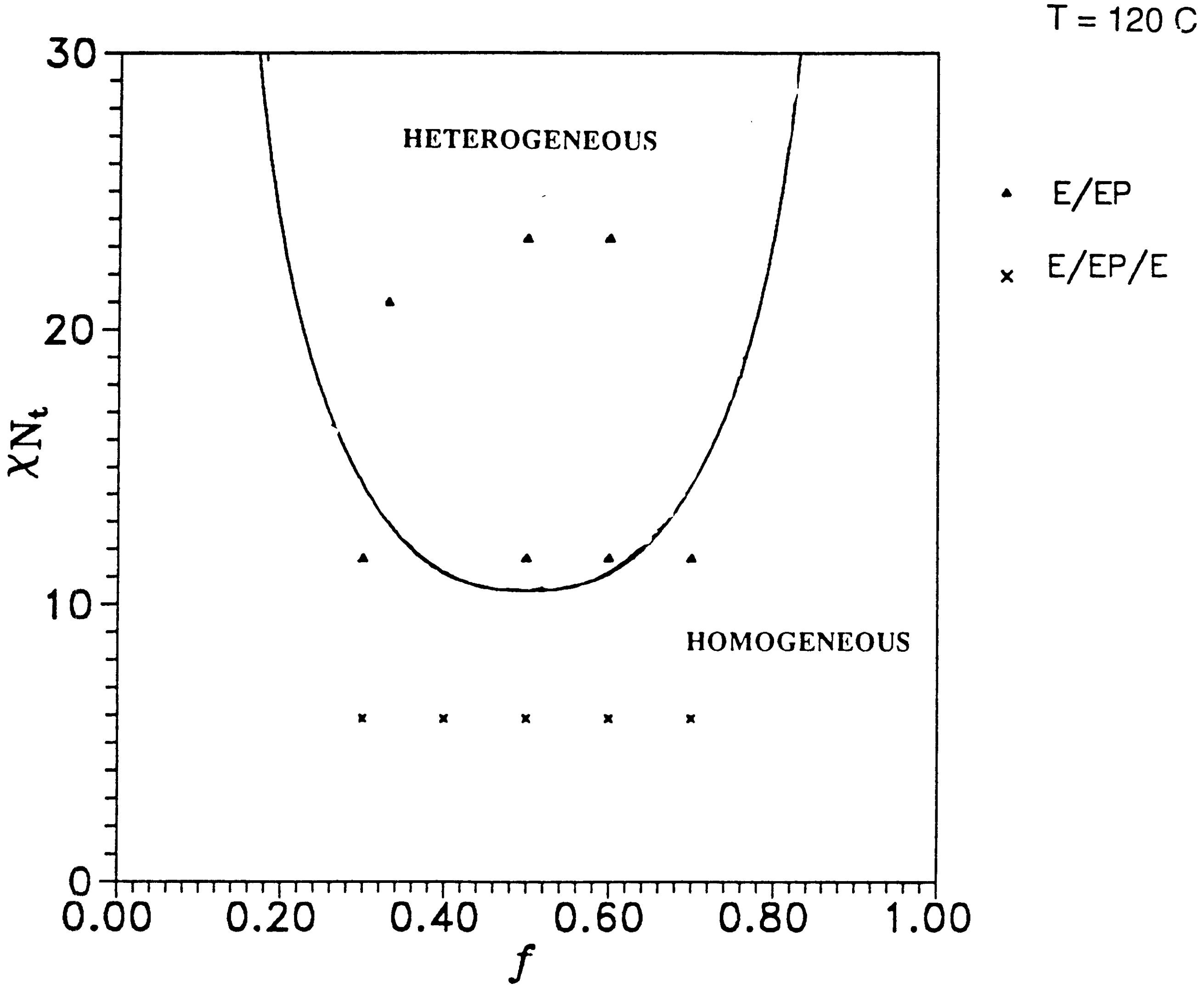

Low frequency dynamic shearing corresponds to low applied stress processing for our channel die experiments, since the higher applied stress on the channel die, the faster the piston moves to compress the polymer sample inside the die. Similarly, high frequencies in the dynamic shearing mode correspond to high applied stresses and perpendicular lamellae morphologies to the plane of shear.

The peculiar perpendicular lamellar orientation was attributed [11] to the disordering ('melting') of the lamellae with immediate regrowth. The thermodynamic barrier to disordering was overcome only near the ODT, thus production of perpendicular lamellae only occurs near the ODT [11]. We find the same behavior here for the case of plane strain compression of our 100 K specimens at 150 °C. We therefore conclude that our E/EP and E/EP/E block copolymers form ordered heterogeneous melts under the shear field imposed from the channel die, when deformed at 150 °C above the E block melting point. As the sample is cooled under load the perpendicular lamellar phase is subsequently 'frozen -in' at the onset of crystallization. The crystallization therefore is required to occur in the presence of this pre-existing lamellar morphology, a situation which has already been shown [7] [8] clearly to lead to the type of unit cell orientation (chains perpendicular to the lamellar normals) shown in Figure 4-10.

The deformation mechanisms involved in producing the channel die samples below the E block melting point, which result in a 'parallel lamellar' morphology, are mostly crystallographic in nature [54], similar to those found in the sub T_m plastic deformation of many polycrystalline materials. The crystallized E chains are once again always perpendicular to the normals of the lamellar superstructure, but in this case the crystallographic texture is deformation-induced unlike the interface dominated crystallization of confined chains mentioned above.

Although the long period spacings of the higher molecular weight samples precluded direct observation of lamellar orientation for these materials, we still may conclude that the channel die processing did not produce any oriented lamellar morphology upon plane strain compression at 150 °C of the E/EP 60/120 100/100 and 120/80 diblocks. This statement is based on the absence of any orientation in the pole figures of these samples. Thus, for the case of semicrystalline block copolymers, the determination of of the unit cell texture via the WAXS pole figure analysis provides an added probe for determining what has happened to the material processed in the melt.

Chapter 5

Gas transport experiments and permeability modeling

5.1 Spherulitic diblock E/EP systems

Gas molecules are generally taken to be insoluble in polymer crystallites and, therefore, are unable to permeate through them [60]. Thus, gas permeation in semicrystalline polymers is essentially confined to the amorphous regions. The crystallites reduce the permeability by decreasing the volume of polymer available for penetrant solution and by constraining the transport along irregular tortuous paths between the crystallites. The reduction in permeability (P), which is the product of the effective diffusion (D) and solubility (S) coefficients, will thus be proportional to the volume fraction of the crystalline phase [61] when all samples have a random misoriented morphology.

The permeation results for the entire series of misoriented spherulitic diblocks as well as for the EP homopolymer are shown in Table 5.1. As expected, these materials have rather low permeabilities, which decrease with increasing crystallinity (increasing amount of E block). From the comparison of the P values for specimens containing the same percentage of E in the EP diblock (E/EP 50/50 and E/EP 100/100, E/EP 120/80 and E/EP 60/40), it is apparent that the permeability is independent of the total molecular weight of the polymer.

GAS	EP 100	E/EP 30/70	E/EP 60/120	E/EP 50/50	E/EP 100/100
He	78.1	33.5	32.0	17.6	18.6
CH_4	29.2	13.5	16.4	9.9	8.8
CO_2	117.0	72.7	51.8	46.7	44.2
N_2	22.3	3.9		3.4	3.9
O_2	37.5	16.5	13.4	8.9	10.6

GAS	E/EP 120/80	E/EP 60/40	E/EP 70/30	E*	E†	LDPE‡
He	16.3	17.2	13.6	6.5	15.7	4.9
CH_4	14.5	10.6	8.7	6.9	13.0	2.9
CO_2	39.5	38.4	36.6	25.5	48.4	12.7
N_2	3.7	2.2	1.9			
O_2	11.5	11.2	7.8	6.9	11.3	2.9

Table 5.1: Permeability coefficients for spherulitic specimens at 25 °C, P in barrers.
* Value for E extrapolated from fit to data.
† Hydrogenated Butadiene, crystallinity 29%, $\rho = 0.894 \frac{g}{cm^3}$
‡ LDPE, $\rho = 0.914 \frac{g}{cm^3}$

The permeability value for the E block lamellae also appears in Table 5.1. These values were not measured directly but were obtained from extrapolations of the fits (nonlinear fitting routine FMINS of the commercially available software package MATLAB shown in Appendix C.2) to the permeability data for the series of diblocks of varying E-block content (Figure 5-1); although the E lamellae contain internal structural complexities of chain folding, amorphous fractions and the like, all of these details are lumped into a quasi-homogeneous material parameter P_E, the effective permeability of the polyethylene - like material in the E domains of the E/EP diblocks. Justification of this simplification will be demonstrated below.

Figure 5-1: Permeability versus %E, spherulitic specimens

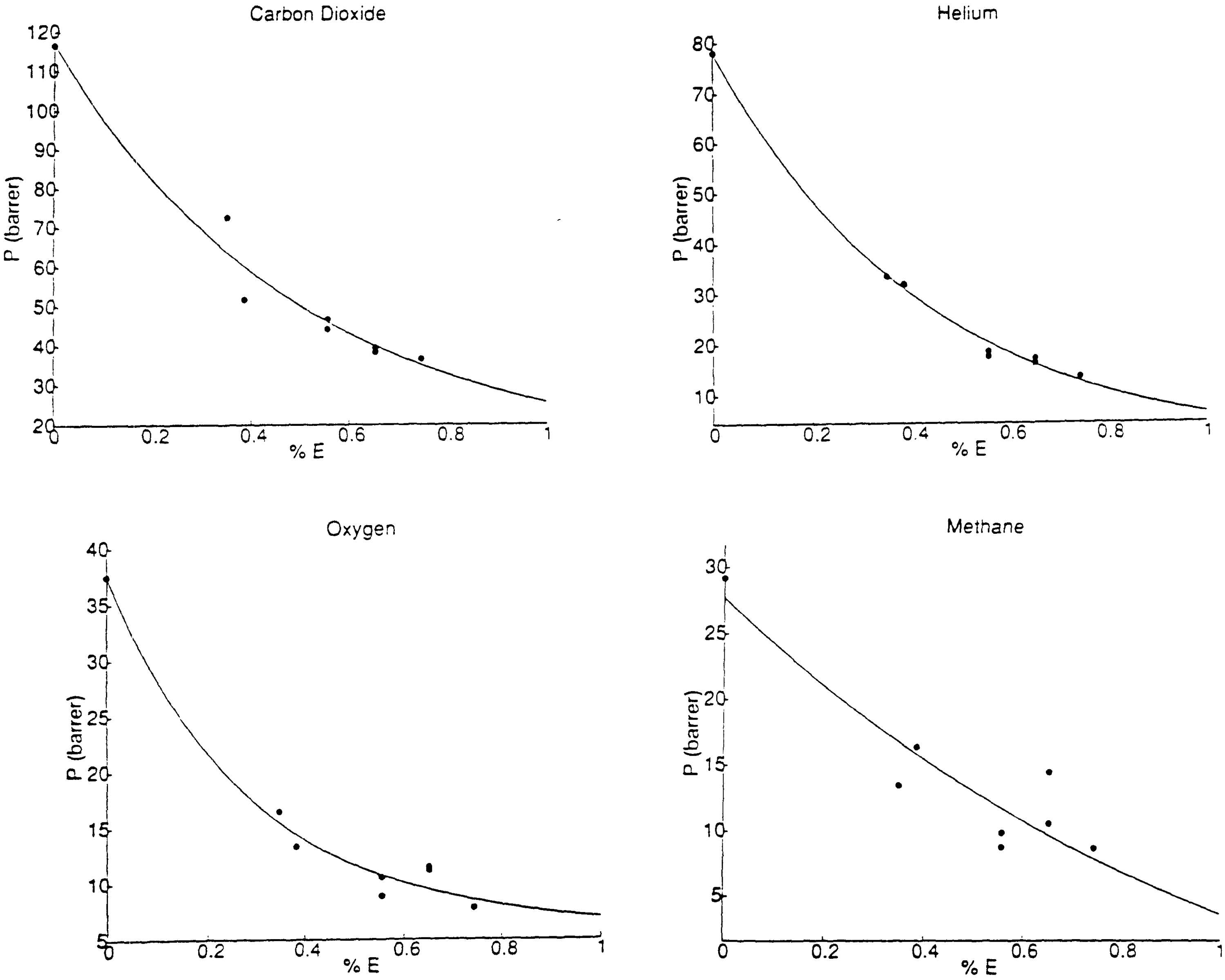

5.2 Modeling of gas transport

The morphology of the E block in any phase-separated E/EP diblock copolymer differs from the morphology of a homopolymer of E, because of the topological constraint imposed at the junction between the two blocks in the diblock copolymer. Since even the slightest morphological differences between two materials can result in big variations in their gas permeability characteristics, P of an E homopolymer for a specific gas does not correspond to P of an E block in the E/EP diblock. The permeability value for the E block was therefore extrapolated from the experimental data, rather than measured from an actual specimen; values of the E block permeability appear in Table 5.1. For all gases, these values fall inbetween the values of permeability for a typical low density polyethylene ($\rho = 0.914\frac{g}{cm^3}$) [62] and of a hydrogenated polybutadiene($\rho = 0.894\frac{g}{cm^3}$) [62], as shown in Table 5.1. On the other hand, the EP homopolymer is considered to be 100% amorphous; hence in this case P of the EP block in an E/EP copolymer can be taken to be the same as of the EP homopolymer, which was determined experimentally.

The effect of microphase orientation on gas permeability is significant. Permeability coefficients for a film whose microdomains are oriented normal to the film surface (parallel to the permeation direction), are much higher than for a film having its microdomains oriented in the same plane as the film surface (in series with respect to the permeation direction) [5]. The resulting expressions for parallel and series laminates for the case of the E/EP diblock copolymers are:

$$P_{par} = P_E v_E + P_{EP} v_{EP} \tag{5.1}$$

$$P_{ser} = \frac{P_E P_{EP}}{P_E v_{EP} + P_{EP} v_E} \tag{5.2}$$

where P_E, P_{EP} = permeability coefficient for the E and EP blocks respectively.

The values of the effective permeabilities of the E (fit) and EP (measured) blocks, were used in the construction of a model predicting gas transport behavior in misoriented heterogeneous polymer systems. This *random column model* has already been successfully applied to a polystyrene - polybutadiene diblock copolymer system [4]. Its validity is now examined for diblock copolymers which contain one block that is crystallizable.

The morphology of the sample is modeled as columns of cubical cells, with each column extending directly from one surface of the film to the other. Each cell contains alternating parallel lamellae which possess a direction of orientation defined by a random angle θ [4]. A periodic boundary condition is imposed at the left and right sides of the cell so that any gas that 'leaves' through either side of the cell as it travels parallel to the orientation direction reenters at the opposing side. It is assumed that the permeating species will preferentially diffuse parallel to the lamellar orientation in each cell. The effective permeability for each cell can be defined as the permeability for a parallel lamellar system, divided by a path length or tortuosity factor τ, which will change from cell to cell. The tortuosity accounts for the fact that a lamellar alignment angle θ other than zero increases the path length a diffusing molecule must travel in order to reach the cell i+1 below:

$$P_i = \frac{P_{par}}{\tau_i} \tag{5.3}$$

$$\tau_i = \frac{1}{cos\theta_i} \tag{5.4}$$

An important constraint imposed on P_i is that a cell's permeability coefficient cannot be lower that that given by the series representation , equation 5.2. If the tortuosity of a cell is so large that the permeability calculated by equation 5.3 is lower than that for the series model, the series value is assigned as the permeability for that cell. The diffusing species is thus allowed to 'choose' the faster of the two modes through any cell, and the effective permeability of the entire column is obtained with the summation *in series* of the individual P_i for each cell:

$$\frac{1}{P_{eff}} = \frac{1}{N}\sum_{i=1}^{N}\frac{1}{P_i} \tag{5.5}$$

where N= number of cells in the column.

A computer simulation obtaining the average *P* of 10,000 columns with N=10,000 cells each has been carried out for He, CO_2, CH_4 and O_2 for all compositions (see Appendix C.2. The number of columns and cells in each column, were chosen to be large enough so that the variations in the permeability coefficient calculated from each run would be minimized. The standard deviation in the *P* values calculated from each simulation was thus reduced to ± 0.1 barrers. The values of θ_i for each cell were calculated using a random number generator. Figure 5-2 shows a plot of P versus number of cells and columns. It is evident as N increases, that above N x N = 1000 x 1000 there is no variation in the *P* values, thus the value of 10000 x 10000 chosen for the simulation is more than adequate to describe a purely random spherulitic specimen.

The predictions of the *random column model* for the permeability coefficients of a randomly oriented sample, are shown in Table 5.2. The agreement between experiment (Table 5.1) and model (Table 5.2) is quite good.

GAS	E/EP 30/70	E/EP 60/120	E/EP 50/50 E/EP 100/100	E/EP 60/40 E/EP 120/80	E/EP 70/30
He	29.0	27.3	20.5	17.2	14.1
CH_4	16.0	15.3	12.4	10.9	9.7
CO_2	62.1	59.2	47.5	41.8	36.8
O_2	18.6	17.7	13.9	12.2	10.6

Table 5.2: Model prediction of *P* for spherulitic specimens at 25 °C from the *P* values of the individual block species

The good agreement between model and measurement also serves to justify our simplification of permeation in the crystallizable E lamellae as described by a single parameter P_E. The fact that the random column model works well for a series of gases, whose ratio of permeabilities EP to E varies from 4 to 12, demonstrates convincingly its ability to simulate the gas transport behavior of these semicrystalline block copolymers over a wide range of permeabilities.

Figure 5-2: Model predictions of permeability versus number of cells and number of columns, He in E/EP 30/70

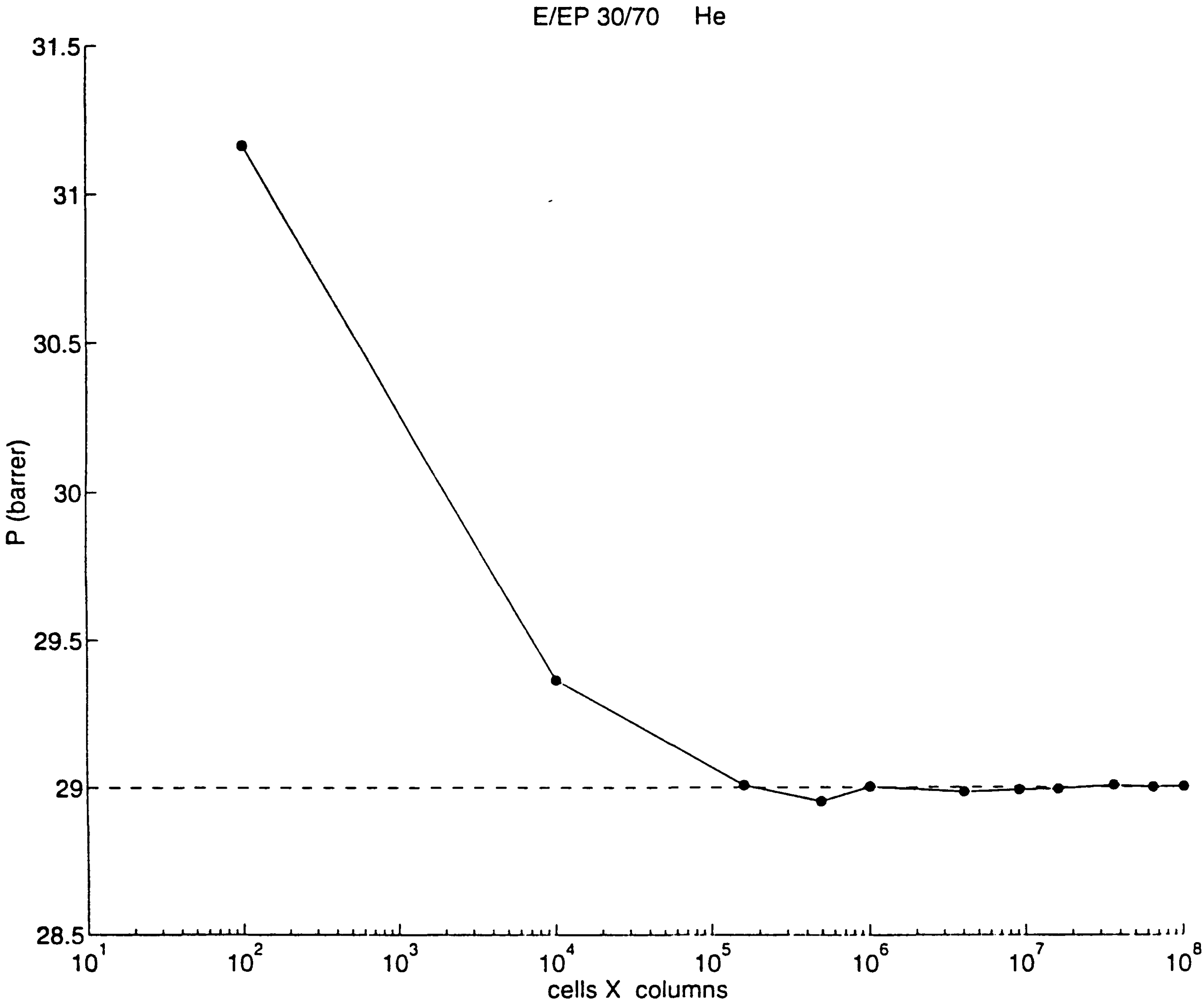

5.3 Plane strain compressed E/EP and E/EP/E systems

The permeation of the E/EP 50/50 specimen with the lamellae aligned in parallel with respect to the permeation direction was measured and is reported in Table 5.3. A large enough pinhole and crack-free specimen of the series lamellar type suitable for gas transport measurements could not however be successfully prepared with the E/EP diblocks.

The values for P_{par} calculated from the model for the E/EP 50/50 polymer, are compared in Table 5.3 to experimental measurements of P_{par} in the plane strain compressed sample. The parallel model (Equation 5.1) is in very good agreement with the experimentally measured value of P_{par}.

GAS	$P_{par}(exp)$	$P_{par}(model)$
He	37.2	38.3
CH_4	15.6	16.8
CO_2	63.3	66.1
O_2	20.5	20.9
N_2	11.5	12.5

Table 5.3: E/EP 50/50 model prediction of P_{par} compared to experimental measurements

The permeation of the E/EP/E 25/50/25 specimen with the lamellae aligned in parallel(P_{par}) and in series (P_{ser})with respect to the permeation direction was measured and is compared in Table 5.4 with the permeability values P_{sph} of the spherulitic specimen and the 'random column ' model predictions.

GAS	$P_{ser}(exp)$	$P_{ser}(model)$	$P_{sph}(exp)$	$P_{sph}(model)$	$P_{par}(exp)$	$P_{par}(model)$
He	12.2	10.9	22.5	20.5	36.2	38.3
CO_2	40.8	39.0	48.3	47.5	62.4	66.1

Table 5.4: Permeability coefficients for E/EP/E 25/50/25

The model slightly underpredicts the experimental value of P_{par} for all gases studied, for both the E/EP 50/50 and the E/EP/E 25/50/25 samples. We cannot expect to construct experimentally a specimen with all of its lamellae being perfectly oriented parallel to the permeation direction ; there will always be some tortuosity in the lamellae, which will reduce the effective permeability of the specimen. We note, however, that this level of agreement between the upper bound model and the near parallel experimental material suggests that the input (extrapolated) values of P_E for each gas represent a very good approximation to the experimentally inaccessible permeation behavior of the semicrystalline E-block domains of the various diblock copolymers. The same argument hold for the model's overprediction of the experimental value of P_{ser} for the triblock E/EP/E 25/50/25 specimen. The perfect 'series' specimen should have the lowest permeability, any other experimentaly manufactured specimen should have higher gas permeability.

The predictions of the respective models for the parallel and series morphologies for each diblock specimen studied are presented in Table 5.5; this is an indication of the upper and lower bounds to gas permeability that can be achieved with each specimen for the gases studied.

GAS	E/EP 30/70		E/EP 60/120		E/EP 50/50 E/EP 100/100		E/EP 60/40 E/EP 120/80		E/EP 70/30	
	P_{par}	P_{ser}	P_{par}	P_{ser}	P_{par}	P_{ser}	P_{par}	P_{ser}	P_{par}	P_{ser}
He	53.1	16.1	50.5	14.9	38.3	10.9	31.4	9.5	24.8	8.4
CH_4	21.4	13.7	20.6	13.0	16.8	10.4	14.7	9.4	12.6	8.6
CO_2	85.1	51.9	81.8	49.1	66.2	39.0	57.3	35.0	48.8	31.8
O_2	26.8	14.7	25.7	13.9	20.5	10.8	17.6	9.6	14.7	8.7

Table 5.5: Model predictions of P_{par} and P_{ser} for the E/EP diblocks

Chapter 6

Summary

It has been demonstrated by the 2-D SAXS spectra that two distinct lamellar orientations can be produced when a series of semicrystalline E/EP and E/EP/E block copolymers of varying E block content and 100,000 g/mole total molecular weight are subjected to high levels of plane strain compression. When the diblocks are deformed above the E block melting point at various compression ratios, the lamellae orient perpendicular to the plane of shear, while texturing below the melt causes the lamellae to orient parallel to the plane of shear. The E/EP/E triblocks exhibit either lamellar orientation when textured above the E block melting point depending on the applied stress on the channel die during deformation.

The morphology produced above the melting point for the E/EP and E/EP/E systems was attributed to proximity of the order-disorder transition to the processing temperature. Although several examples of the unexpected perpendicular orientation have been reported for amorphous diblock copolymers, this is the first experimental documentation of perpendicular orientation in sheared semicrystalline block copolymer lamellar phases. The semicrystalline diblocks and triblocks exhibit the perpendicular lamellar orientation for a much broader composition range than any amorphous diblock system reported to date. Furthermore, the semicrystalline systems offer the advantage that the crystallographic texture, which is eventually locked into the materials when cooled below T_m, provides an independent set of clues regarding the orientation of the lamellae at the point when crystallization takes place. Conversely, the deformation mechanisms at T < T_m, which lead to the series lamellar morphology, are crystallographic in nature. WAXS pole figure analysis has revealed that the orientation of the crystallized E chains is perpendicular to the lamellar normal, irrespective of the deformation temperature. When the processing is carried out above T_m, the heterogeneous melt orients perpendicular to the shear planes and then upon cooling the E block chains crystallize within the amorphous lamellar microdomains, a process which has been shown to generate a crystallographic texture with chains perpendicular to the lamellar normals [7] [8].

A simple model of gas permeation in misoriented lamellar materials successfully describes the permeation behavior of the spherulitic E/EP diblock copolymers for a wide range of compositions. The model assumes that the majority of the transport takes place along the more conductive, amorphous EP lamella but recognizes the smaller, but non zero, permeability of the semicrystalline E domains. The observed lowering of the permeability of the copolymer by the presence of these semicrystalline E regions is accounted for in the model through considerations of its volume fraction and through an effective tortuosity which is introduced into the materials. Values of P_{EP} could be determined directly via gas permeation measurements on the corresponding EP amorphous homopolymer; however, the permeation behavior of the semicrystalline E domains could not be obtained in a similar fashion because their internal structural details [7] are different from the spherulitic texture of the corresponding E homopolymer, due to the topological constraint imposed at the junction of the E and EP blocks in the E/EP diblock copolymer. Therefore P_E values were obtained by extrapolation of permeation data for a series of copolymers of varying E-block content.

The excellent agreement between the random column model and experiments in the E/EP and E/EP/E plane strain compressed materials, suggests that permeabilities of other spherulitic semicrystalline diblock copolymers can be anticipated without need for synthesizing every candidate system under consideration. The upper and lower bounds (parallel and series) models represent the limiting cases for high throughput or good barrier membranes, respectively. The oxygen permeability of butyl rubber, a barrier elastomer, is 2.1 barrers [63]. This value is not dramatically lower than the predicted value of 8.7 barrers for the series E/EP 70/30 material (Table 5), thus suggesting possible uses of the E/EP diblocks as barrier materials in certain applications. We also note that the superficial mechanical properties (stiffness versus flexibility) depend greatly on the volume fraction composition of the E/EP diblocks, which represents another possible degree of freedom in membrane design using these materials.

Appendix A

Optical Micrographs of Spherulitic E/EP and E/EP/E

10µm [illegible] HP[illegible] [illegible] AT 70 [illegible] FROM MELT

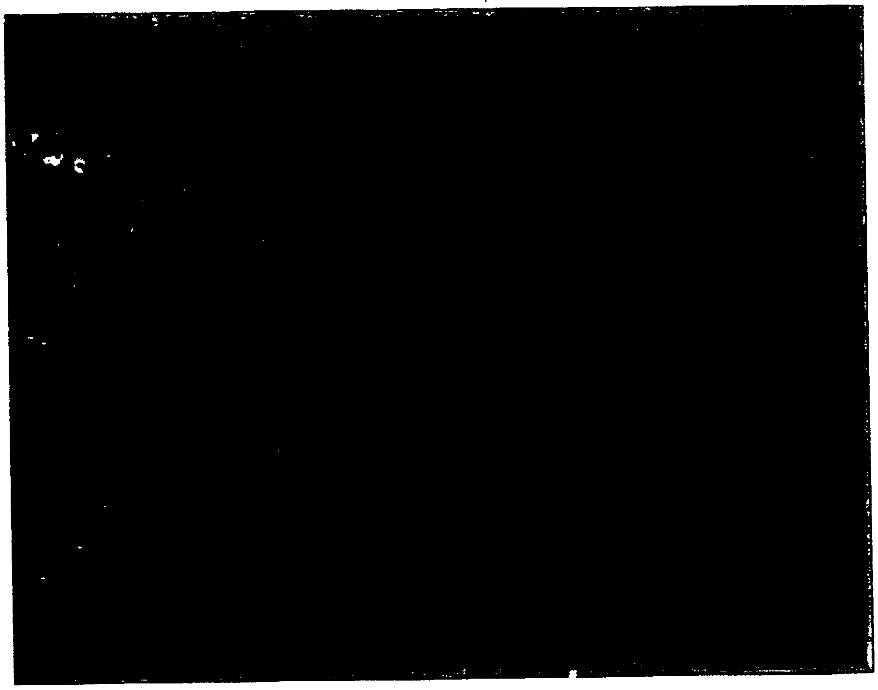

HPB 90K/HPI 30K CRYSTALLIZED AT 80°C FROM MELT

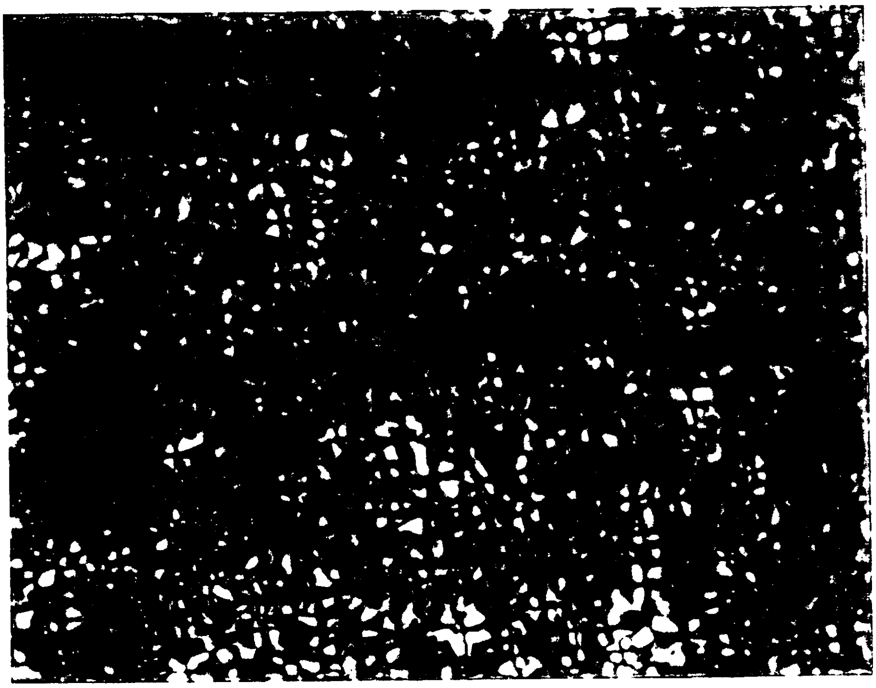

[illegible] [illegible] FROM MELT 10 μm

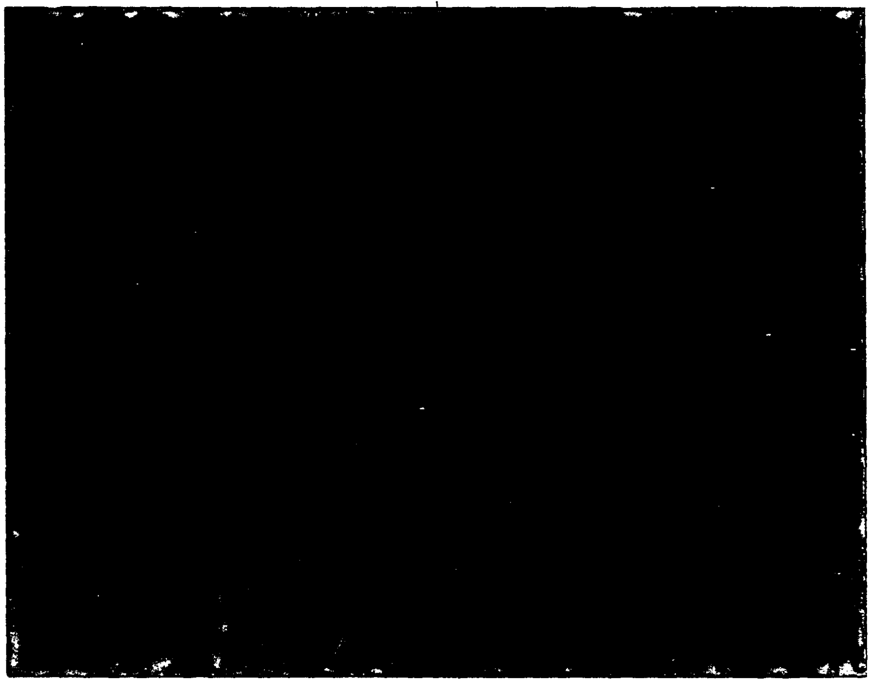

10 μm [illegible] SLOW COOLED FROM MELT [illegible]

Appendix B

Averaged SAXS spectra of channel die E/EP above T_m

E/EP 70/30

LD

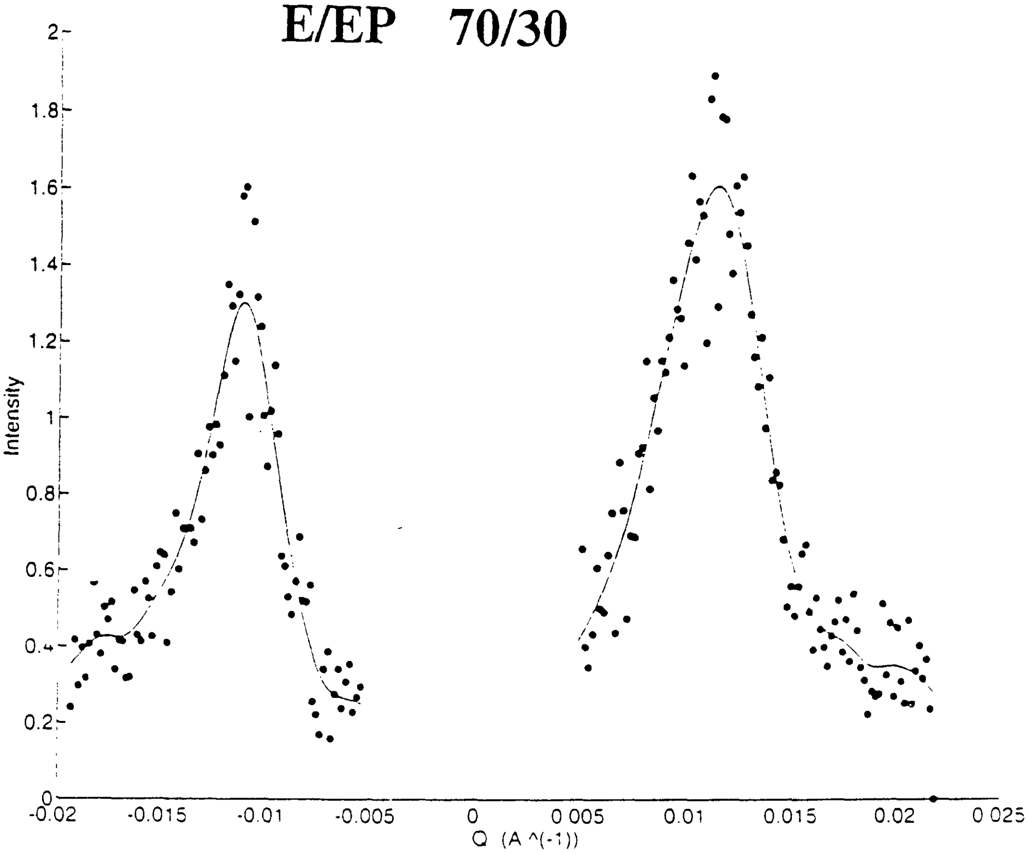

FD

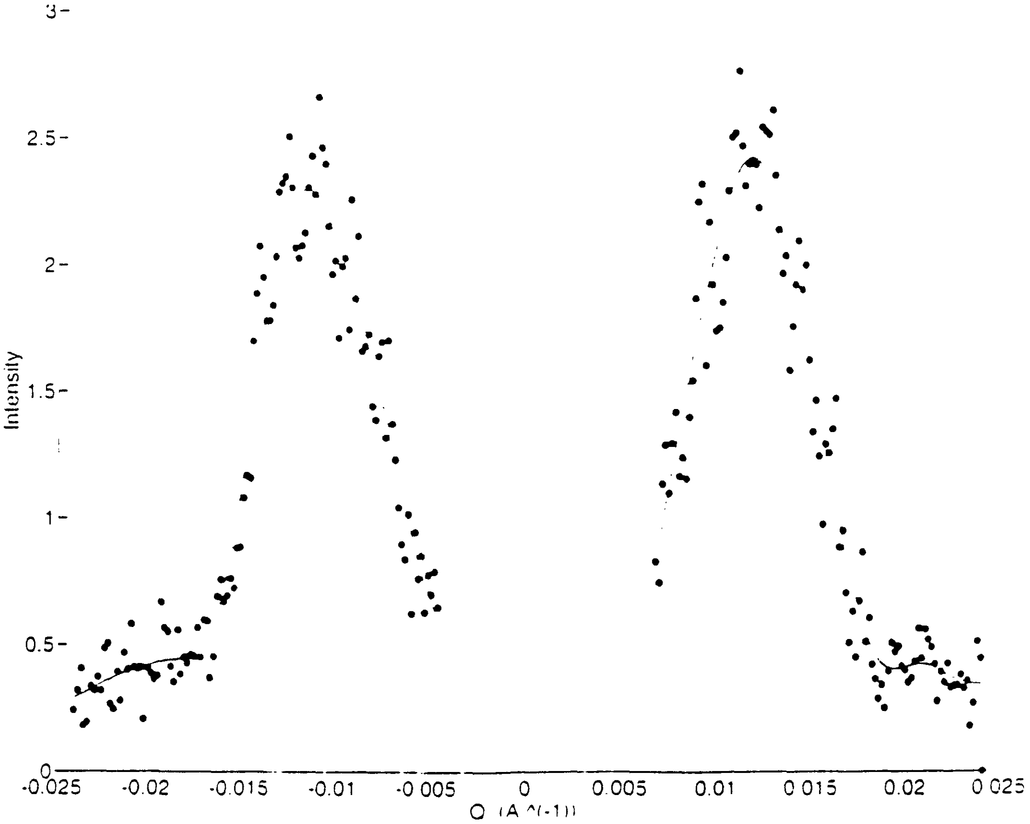

E/EP 50/50

LD

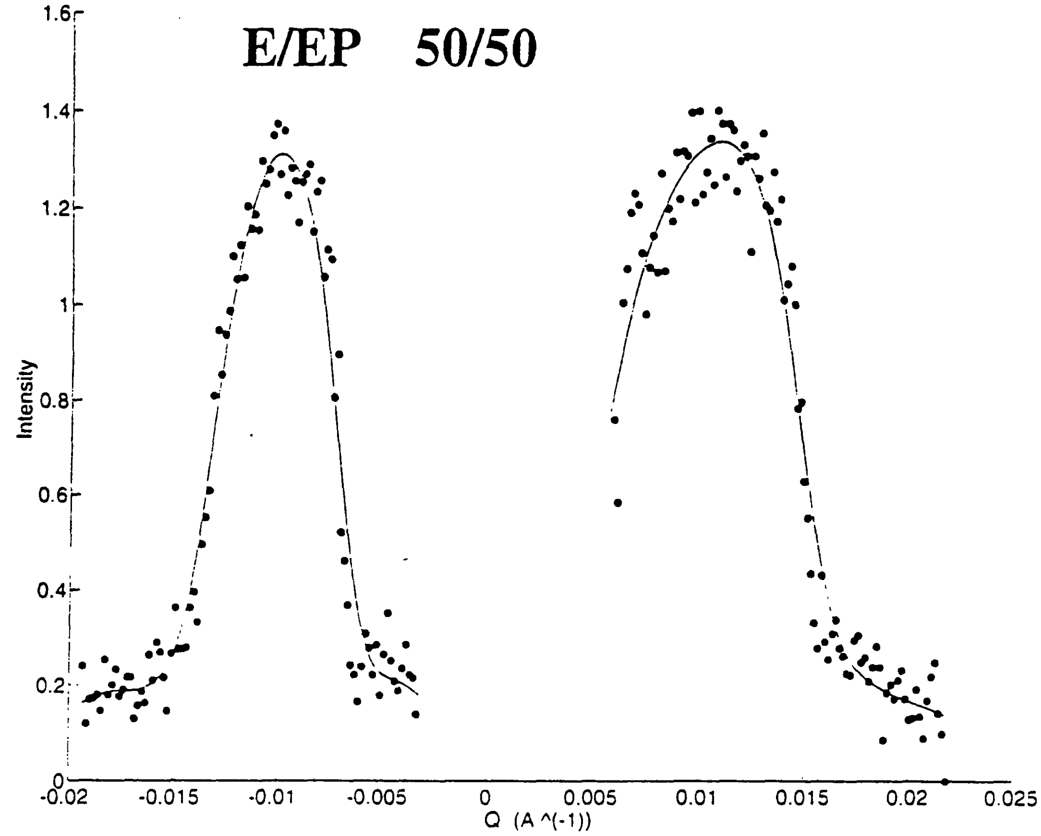

FD

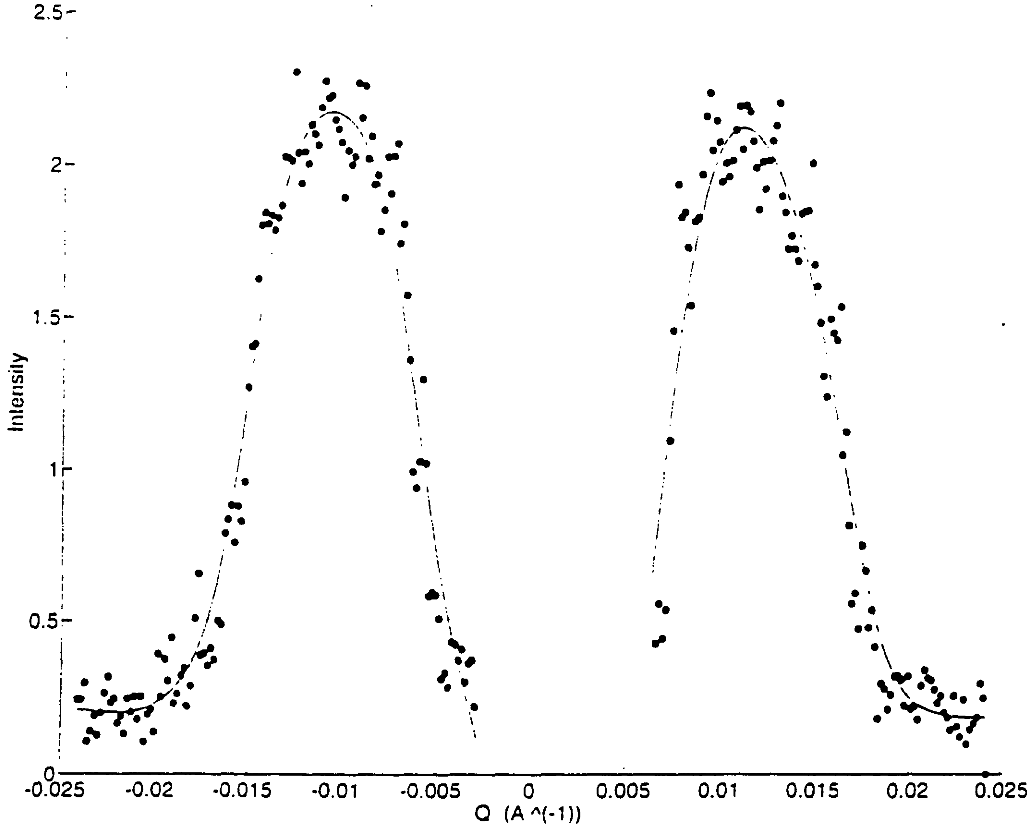

E/EP 30/70

LD

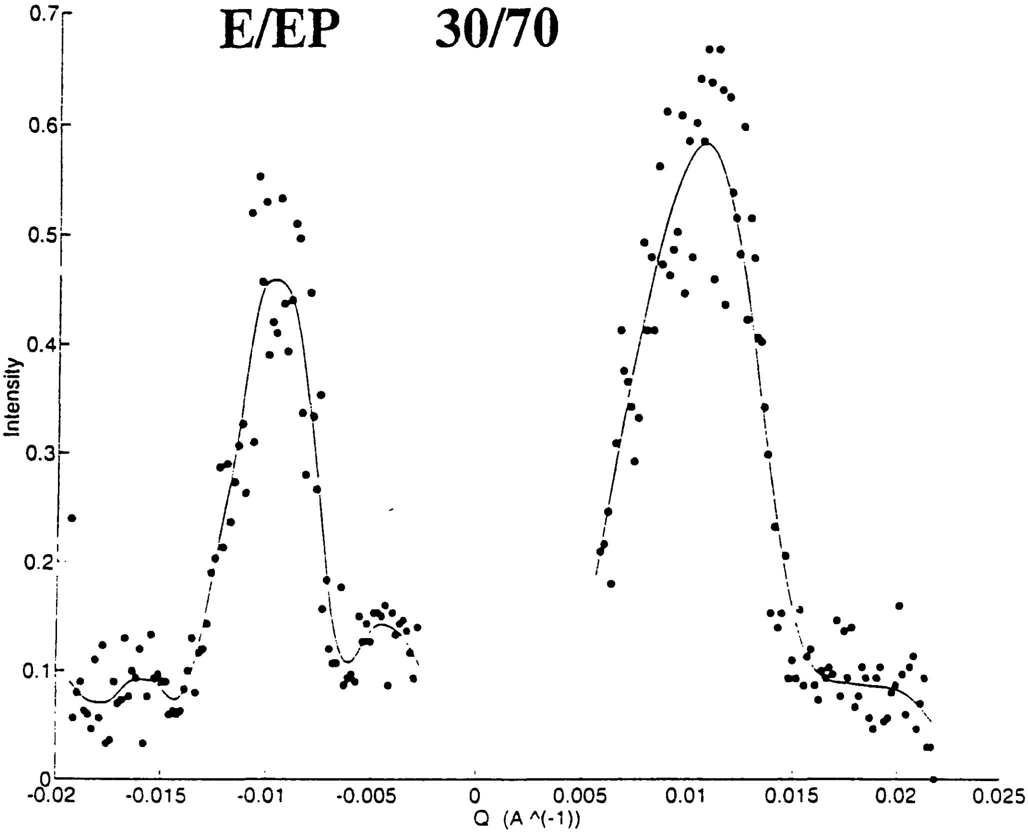

FD

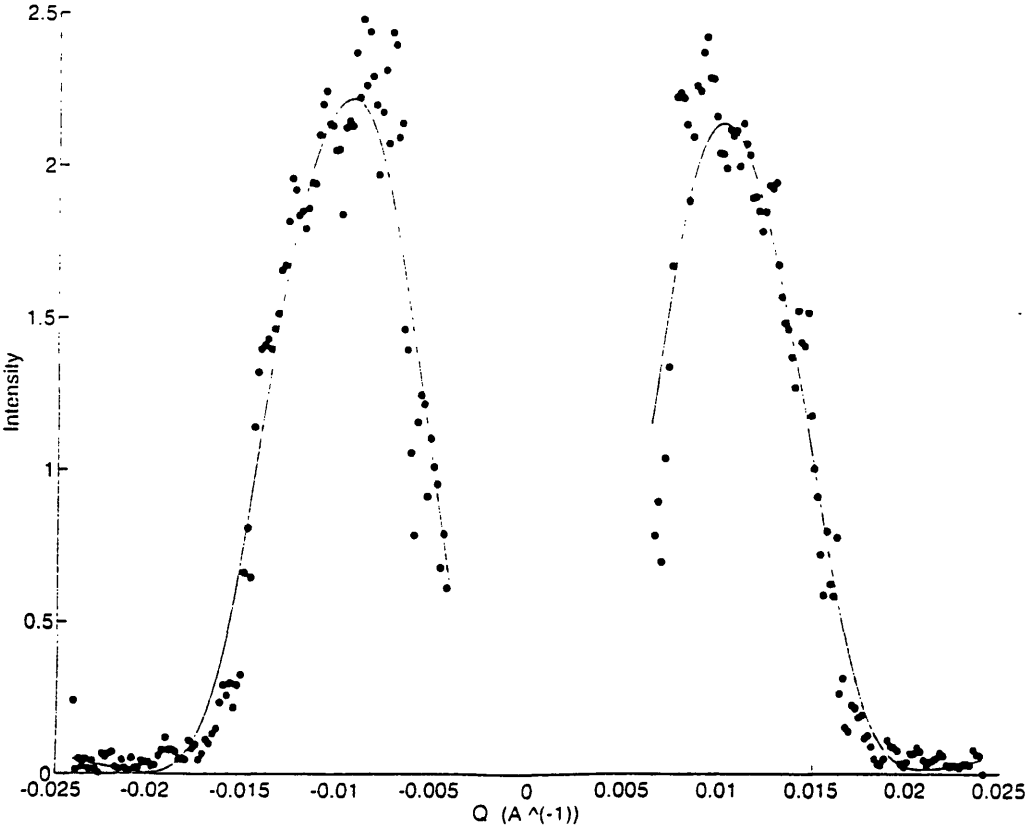

Appendix C

Computer Codes

C.1 X-ray Programs

```
function [out,outs,d] = saxsrandom(tst,factor, time,jj1);
% **************      SAXSRANDOM  **********************
% [out,outs,d] = saxsrandom(tst,factor, time,jj1);
% Stores file in I vs Q format DOES EVERYTHING, SMOOTHING, etc
%        tan (2theta) =#pixels / factor
% TIME = collection time in seconds, TST= original *.tst data
% JJ1= Smoothing Factor
% JR= Smoothing Factor for RIGHT side of data
%  RECOMMENDED VALUE: JJ1=6 (>6 gives more smoothing
% (I vs Q) are the outputs out=original, outs=splinefit
%
% LAST MODIFIED : 11/6/93
%@C Peter Kofinas

% Make two column data
tst1=plottst(tst);

% Some useful constants and initializations

pi2=2*3.14159;
q1=2*pi2/1.54;
k=1;
le2=length(tst1);

for i=1:le2;
     out(i,1)=sin(atan(tst1(i,1)/factor)/2)*q1;
     out(i,2)=tst1(i,2)/time;
end;

% Call program to calculate and plot results

[outs,d]=plotsaxs(out,jj1);
end
```

```
function [out,outs,d] = saxsorient(tst,factor, time,jl,jr);
%  ******  SAXSORIENT***********
% [out,outs,d] = saxsorient(tst,factor, time,jl,jr);
% Stores file in I vs Q format DOES EVERYTHING, SMOOTHING, etc
%        tan (2theta) =#pixels / factor
% TIME = collection time in seconds, TST= original *.tst data
% Jl= Smoothing Factor for LEFT side of data
% JR= Smoothing Factor for RIGHT side of data
%  RECOMMENDED VALUE: JL=JR= 5 (>5 more smoothing)
% (I vs Q) are the outputs out=original, outs=splinefit
%
% LAST MODIFIED: 9/26/93
% WRITTEN BY: PETER KOFINAS

% Make two column data
tstnew=plottstor(tst);

% Plot the raw data

h=plot(tstnew(:,1),tstnew(:,2),'.y');
get(h);
set(h,'MarkerSize',15);
set (gca,'Box','of')
hold on;
plot(tstnew(:,1),tstnew(:,2),'r');
hold off;
xxx= ['click on peak pairs, left to right ']
xxx= ['Then press < Return > on graph screen ']
[x,y]=ginput;
center=findcenter(x);
zeropoint=find(tstnew(:,1) == center);
le=length(tstnew);

%Now plot data in I vs Q format

pi2=2*3.14159;
q1=2*pi2/1.54;
for i=1:le;
     out(i,1)=sin(atan((tstnew(i,1)-zeropoint)/factor)/2)*q1;
     out(i,2)=tstnew(i,2)/time;
end;
[outs,d,point,points]=plotsaxsor(out,jl,jr);
end
```

```
function out1 = plottst(tst);
%  ******  PLOTTST***********
% OUT1=PLOTTST(TST) makes a 2-d matrix out1 of the
% *.tst raw file for RANDOM SAXS DATA. Plots Intensity vs pixel position
%  Also Deletes beamstop points
%
% LAST MODIFIED: 11/6/93
% WRITTEN BY: PETER KOFINAS

clf reset;
len=length(tst)-1;
k=1;
% Make 2 x 2 matrix out, 1st col=pixel, 2nd col=counts
for i=1:2:len;
  out(k,1)=k;
  m=i+1;
  out(k,2)=tst(m,1);
  k=k+1;
end;
l=length(out);
plot(out(1:l,1), out(1:l,2), out(1:l,1), out(1:l,2),'oy');
'Rescale the axes manually so you can see the peaks'
tt1=1;
while(tt1==1);
  tt1=input('Use other axes? (1=yes)    ');
  tt2=input('Input axis values in the form [xmin xmax ymin ymax]');
  axis (tt2);
end;
pp2=['Click on last beamstop data point with mouse:']
pp2=[' then type <Return> on the graph screen']
[x,y]=ginput;
x1=round(x);
out(1:x1,2)=zeros(x1,1);
out1=out(x1+1:tt2(2),:);
plot(out1(:,1), out1(:,2), out1(:,1), out1(:,2),'oy');
end
```

```
function out1 = plottstor(tst);
%  ******  PLOTTSTOR***********
% OUT1=PLOTTSTOR(TST) makes a 2-d matrix out1 of the
% *.tst raw file for ORIENTED SAXS DATA. Plots Intensity vs pixel position
% Also Deletes beamstop points
%
% LAST MODIFIED: 11/6/93
% WRITTEN BY: PETER KOFINAS

clf reset;
len=length(tst)-1;
k=1;
% Make 2 x 2 matrix out, 1st col=pixel, 2nd col=counts
for i=1:2:len;
  out(k,1)=k;
  m=i+1;
  out(k,2)=tst(m,1);
  k=k+1;
end;
l=length(out);
plot(out(1:l,1), out(1:l,2), out(1:l,1), out(1:l,2),'oy');
'Rescale the axes manually so you can see the peaks'
tt1=1;
while(tt1==1);
  tt1=input('Use other axes? (1=yes)   ');
  tt2=input('Input axis values in the form [xmin xmax ymin ymax]');
  axis (tt2);
end;
pp2=['Click on beamstop data range with mouse:']
pp2=[' first left (xmin) then right (xmax)']
pp2=[' then type <Return> on the graph screen']
[x,y]=ginput;
x1=round(x(1)); x2=round(x(2));
out(x1:x2,2)=zeros(x2-x1+1,1);
out1=out(tt2(1):tt2(2),:);
plot(out1(:,1), out1(:,2), out1(:,1), out1(:,2),'oy');
end
```

```
function out=findcenter(x);
% ************  FINDCENTER********************
% CENTER=FINDCENTER(x) finds center of data .  Run plottst first
%[x,y]=ginput => get pixel values for peak(s), need only X = pixel
%numbers.  X1,X2 are peak pairs, X3,X4 next pair, etc.
%
% LAST MODIFIED: 9/26/93
% WRITTEN BY: PETER KOFINAS

len=length(x);
k=1;
for i=1:2:len-1;
 outs(k)=round((x(i)+x(i+1))/2);
 k=k+1;
end;
out=mean(outs);
end
```

```
function dmean=dspacing;
% ******************   DSPACING   *************************************
% Finds long period D from x-ray graph.  Must be in I vs Q format.
% Choose 2 peaks of graph put the crosshair on each peak, then click
% on the left mouse button and press return.  Only the Q value is important.
%
% LAST MODIFIED: 8/24/93
% WRITTEN BY: Peter Kofinas

[x,y]=ginput;
d(1)=round(2*pi/x(1))
d(2)=round(2*pi/x(2))
dmean=round(mean([abs(round(2*pi/x(1))) abs(round(2*pi/x(2)))]))
end
```

```
function [outs,d]=plotsaxs(out,jj1);
% ********************* PLOTSAXS *****************************
% [outs,d]=plotsaxs(out,jj1);
% Plots stored SAXS data uses out j1 from whichspline out from saxs
% outs =smoothed data,
% d=dspacing of max peak
%
% LAST MODIFIED: 9/26/93
% WRITTEN BY: PETER KOFINAS

lee=length(out);
xi=out(:,1)';
dd1= max(diff(xi))*14;
dd2= max(diff(out(:,2)))*0.5;
ee= max(diff(xi))/4;
epsilon = max(diff(xi))^3/16;
xx=out(1,1):ee:out(lee,1);
le2=length(xx);
ybad=out(:,2)';
outs=zeros(le2,2);
j=jj1+3;
yy= csaps(xi,ybad,1/(1+epsilon*3^(j-3)),xx);
outs(:,1)=xx';
outs(:,2)=yy';
tt2=input('Input title of graph (Must be inside quotes) ');
mm=find(outs(:,2)==max(outs(:,2)));
d=round(2*pi/outs(mm,1));
tt1=[tt2 '    D= ' num2str(d) ' A' '      ' date];

% plot the results
figure(1); clf reset;
h=plot(out(:,1),out(:,2),'.y');
set(h,'MarkerSize',16);set (gca,'Box','of');hold on;
le2=length(outs);
gg=plot(outs(1:le2,1),outs(1:le2,2),'r');
set(gg,'MarkerSize',25);
title(tt1);
xlabel(' Q  (A ^(-1)) '); ylabel('Intensity');
orient landscape; hold off;
klik=input('Send to Printer ?  (1=yes) ');
if (klik ==1)
  print -dps;
end;

end
```

```
function [outs,d,point,points]=plotsaxsor(out,jl,jr);
% ********************** PLOTSAXSOR *****************************
% [outs,d,point,points]=plotsaxsor(out,jl,jr);
% Plots stored ORIENTED SAXS data
% uses out from saxs (I vs Q data),  j1 from whichspline
% jj1l=left peak, jj1r=right peak
% outs =smoothed data
% d = dspacing of max peak
%
% LAST MODIFIED: 9/26/93
% @C PETER KOFINAS

% Fit with splines

zeropoint=find(out(:,1)==0);
lee=length(out);
xx1a=find(out(:,2)); xx1b=find(diff(xx1a) ~=1);
x1=xx1a(xx1b)+1; x2=xx1a(xx1b+1)-1;
point=[x1-1 x2+1];
[outsl,dl]=splinefitor(out(1:x1,:),jl);
[outsr,dr]=splinefitor(out(x2:lee,:),jr);
d=round(mean([dl dr]));
dl,dr,d
points=length(outsl);
outt1=[outsl(:,1)' outsr(:,1)']';
outt2=[outsl(:,2)' outsr(:,2)']';
outs=[outt1 outt2];

tt2=input('Input title of graph  (Must be inside quotes) ');
tt4=[ '    jl= ' num2str(jl) ' jr= ' num2str(jr) ];
tt1=[tt2 tt4 '   D= ' num2str(d) ' A' '         ' date];

% plot the results

figure(1); clf reset;
h1=plot(out(1:point(1),1),out(1:point(1),2),'.y');
set(h1,'MarkerSize',16);
set (gca,'Box','of');hold on;
h2=plot(out(point(2):lee,1),out(point(2):lee,2),'.y');
set(h2,'MarkerSize',16);
le2=length(outs);
gg=plot(outs(1:points,1),outs(1:points,2),'r');
set(gg,'MarkerSize',25);
gg1=plot(outs(points+1:le2,1),outs(points+1:le2,2),'r');
set(gg1,'MarkerSize',25);
title(tt1);
xlabel(' Q  (A ^(-1)) '); ylabel('Intensity');
orient landscape; hold off;
klik=input('Send to Printer Cheme0 ?  (1=yes) ');
if (klik ==1)
  print -dps -Pcheme0;
end;
end
```

```
function [outs,d]=splinefitor(out,jj1);
% ********************* SPLINEFITOR ****************************
% [outs,outsp,d]=splinefitor(out1,jj1);
% Spline fit ROUTINE for ORIENTED samples, gets called from plotsaxsor
% Plots stored SAXS data uses j1 from whichspline, out from saxsorient
% outs =smoothed data
% d=dspacing of max peak  ORIENTED DATA
%
% LAST MODIFIED: 10/12/93
% @C PETER KOFINAS

% Fit with cubic splines

lee=length(out);
xi=out(:,1)';
ee= max(diff(xi))/4;
epsilon = max(diff(xi))^3/16;
xx=out(1,1):ee:out(lee,1);
le2=length(xx);
ybad=out(:,2)';
outs=zeros(le2,2);
j=jj1+3;
yy= csaps(xi,ybad,1/(1+epsilon*3^(j-3)),xx);
outs(:,1)=xx';
outs(:,2)=yy';
mm=find(outs(:,2)==max(outs(:,2)));
d=abs(round(2*pi/outs(mm,1)));
end
```

```
function [iqout,iqouts]=iqsquare(out,outs,factor);
% **********   IQSQUARE   *************
% plots SAXS data in I Q^2  vs Q for lamellar data
% [iqout,iqouts]=iqsquare(out,outs,factor);
% Input is after run with saxs or saxsorient programs
% generates new spline fit iqouts, original data output= iqout
% input out=original data from saxs4, outs=splinefit from saxs
%
%  LAST MODIFIED: 9/26/93
%  WRITTEN BY: PETER KOFINAS

le=length(out);
lee=length(outs)-20;
for i=1:le;
qsq=out(i,1)^2;
qsqs=outs(i,1)^2;

iqout(i,1)=out(i,1);
iqouts(i,1)=outs(i,1);

iqout(i,2)=log(out(i,2)/factor)*qsq;
iqouts(i,2)=log(outs(i,2)/factor)*qsqs;
end;
for i=le+1:lee;
qsqs=outs(i,1)^2;
iqouts(i,1)=outs(i,1);
iqouts(i,2)=log(outs(i,2)/factor)*qsqs;
end;

h=plot(iqout(:,1),iqout(:,2),'.y');
xlabel('Q');
ylabel('I*Q*Q');
set(h,'MarkerSize',15);
set (gca,'Box','of')
hold on;
orient landscape;

plot(iqouts(1:lee,1),iqouts(1:lee,2),'r');
hold off
end
```

```
function [outs,jj1]=whichspline(z1);
% ********************** WHICHSPLINE ***********************
% [outs,jj1]=whichspline(z);
%
% Find factor jj1 for best spline fit to data
% Input raw data I vs Q from saxs2, output smoothed data
%
% LAST MODIFIED:  9/23/93
% WRITTEN BY: Peter Kofinas

clf reset;
lee=length(z1);
xi=z1(:,1)';
ee= max(diff(xi))/4;
epsilon = max(diff(xi))^3/16;
xx=z1(1,1):ee:z1(lee,1);
le2=length(xx);
ybad=z1(:,2)';
outs=zeros(le2,2);

% Calculate and  plot the results
for j=4:11;
   clg;
   j1=j-3
   yy(j1,:) = csaps(xi,ybad,1/(1+epsilon*3^(j-3)),xx);
   plot(z1(:,1),z1(:,2),'oy',z1(:,1),z1(:,2),':y',xx,yy(j1,:),'r');
   pl=input('Plot data? 1=yes ');
   if (pl==1);
     p2=num2str(j1);
     title(p2);
     print -dps ;
   end;
end;
jj1=input('Choose 1 to 8 ');
outs(:,1)=xx';
outs(:,2)=yy(jj1,:)';
hold off;
end
```

```
function [outs,jj1]=whichsplineor(z);
% ********************** WHICHSPLINEOR ***********************
% [outs,jj1]=whichsplineor(z);
%
% Find factor jj1 for best spline fit to data
% Input raw data I vs Q from saxs2, output smoothed data
% LAST MODIFIED:  9/23/93
% WRITTEN BY: Peter Kofinas

% Take left half of data
le3=length(z)/2;
z1=z(1:le3,:);
clf reset;
lee=length(z1);
xi=z1(:,1)';
ee= max(diff(xi))/4;
epsilon = max(diff(xi))^3/16;
xx=z1(1,1):ee:z1(lee,1);
le2=length(xx);
ybad=z1(:,2)';
outs=zeros(le2,2);
% Calculate and  plot the results
for j=4:11;
   clg;
   j1=j-3
   yy(j1,:) = csaps(xi,ybad,1/(1+epsilon*3^(j-3)),xx);
   plot(z1(:,1),z1(:,2),'oy',z1(:,1),z1(:,2),':y',xx,yy(j1,:),'r');
   pl=input('Plot data? 1=yes ');
   if (pl==1);
     p2=num2str(j1);
     title(p2);
     print -dps ;
   end;
end;
jj1=input('Choose 1 to 8 ');
outs(:,1)=xx';
outs(:,2)=yy(jj1,:)';
hold off;
end
```

```
function [out,outs] = waxs(tst1,factor, time);
% **************      WAXS  **********************
% RUN first PLOTTST.  Delete zeros  at begining and end of data
% [OUT,OUTS]=WAXS(TST,FACTOR, TIME)
% makes a 2-d matrix out of the test.tst file for
% RANDOMLY ORIENTED samples.
% outs=fitted data with splines .Plots log I vs 2 theta
% factor = from 2theta scan, pick best peak: tan(20)=#pixels/factor
% LAST MODIFIED : 9/15/93
% WRITTEN BY:  Peter Kofinas

% Some useful constants and initializations

le2=length(tst1);

%  Fit data with splines
smooth=splinefit(tst1);
le3=length(smooth);

for i=1:le2;
     out(i,1)=atan(tst1(i,1)/factor)*180/pi;
     out(i,2)=tst1(i,2)/time;
end;

for i=1:le3;
     outs(i,1)=atan(smooth(i,1)/factor)*180/pi;
     outs(i,2)=smooth(i,2)/time;
end;

%plot results
clg;
figure(1);
h=plot(out(:,1),out(:,2),'.y');
xlabel(' 2 Theta ');
ylabel('Intensity');
get(h);
set(h,'MarkerSize',15);
set (gca,'Box','of')
hold on;
orient landscape;
lee=length(outs)-10;
plot(outs(1:lee,1),outs(1:lee,2),'r');
hold off
end
```

```
function [out,outs] = waxsorient(tstnew,factor, time);
%  ******  WAXSORIENT***********
% [out,outs] = waxsorient(tstnew,factor, time);
% Stores file in I vs Q format
%        tan (2theta) =#pixels / factor
% TIME = collection time in seconds
% TSTNEW = output file after "plottst" (can "cleanup" file if you want,
% i.e  remove zeroes from the end, maybe also first couple of points)
% and beamstop data
% factor = from 2theta scan, pick best peak: tan(20)=#pixels/factor
% ONLY NEED original tstfile from "plottst"
% (I vs 2 Theta) are the outputs out=original, outs=splinefit
%
% LAST MODIFIED: 9/15/93
% WRITTEN BY: PETER KOFINAS

% Plot the raw data
h=plot(tstnew(:,1),tstnew(:,2),'.y');
get(h);
set(h,'MarkerSize',15);
set (gca,'Box','of')
hold on;
plot(tstnew(:,1),tstnew(:,2),'r');
hold off;
xxx= ['click on peak pairs, left to right ']
[x,y]=ginput;
center=findcenter(x)
zeropoint=find(tstnew(:,1) == center);
le=length(tstnew);

% Fit with splines
sm1=splinefitor(tstnew,center);

%Now plot data in I vs 2thetaformat
pi2=2*3.14159;
for i=1:le;
out(i,1)=atan((tstnew(i,1)-zeropoint)/factor)*180/pi;
out(i,2)=tstnew(i,2)/time;
end;
lee=length(sm1);
for i=1:lee;
outs(i,1)=atan((sm1(i,1)-zeropoint)/factor)*180/pi;
outs(i,2)=sm1(i,2)/time;
end;
orient landscape;
h=plot(out(:,1),out(:,2),'.y');
ylabel('Intensity');
xlabel('2 Theta');
get(h);
set(h,'MarkerSize',15);
set (gca,'Box','of');
hold on;
plot(outs(:,1),outs(:,2),'r');
hold off;
end
```

```
function [factor,duckout] = ducktendon(tstnew, center, time);
%  ***********DUCKTENDON****************************
% [FACTOR,DUCKOUT]=DUCKTENDON(TSTNEW,CENTER,TIME) finds factor for S-D
% calibration from duck tendon data:
% Stores file in I vs Q format
%        tan (2theta) =#pixels / factor
% TIME = collection time in seconds
% TSTNEW = duck file after "plottst" (can "cleanup" file if you want,
%  i.e  remove zeroes from the end, maybe also first couple of points
%  from beamstop)
% CENTER = center from "findcenter" , original tstfile from "plottst"
% FACTOR, DUCKOUT (I vs Q) are the outputs
%
% LAST MODIFIED: 4/29/93
% WRITTEN BY: PETER KOFINAS

zeropoint=find(tstnew(:,1) == center);
le=length(tstnew);
% first plot as Intensity vs pixels
for i=1:le;
temp(i,1)=tstnew(i,1)-zeropoint;
temp(i,2)=tstnew(i,2);
end;
plot(temp(:,1), temp(:,2),temp(:,1),temp(:,2),'o');
%Now calculate factor and replace pixels with Q data
%Use Peaks 640/2=320, 640/3=213.333 and 640/6=106.67 click on 320 peaks first,
%then 213 left to right
xx= ['click on 320 then 213.33, 106.67  peak pairs, left to right ']
[x,y]=ginput;
pix320=mean([abs(x(1)) abs(x(2))]);
coef320=tan(2*asin(0.77/320));
pix213=mean([abs(x(3)) abs(x(4))]);
coef213=tan(2*asin(0.77/213.33333333));
pix107=mean([abs(x(5)) abs(x(6))]);
coef107=tan(2*asin(0.77/106.6666666667));
fac320=pix320/coef320
fac213=pix213/coef213
fac107=pix107/coef107
factor=0.5*fac107+0.3*fac320+0.2*fac213
save factortime factor time;
%Now plot data in I vs Q format
pi2=2*3.14159;
q1=2*pi2/1.54;
for i=1:le;
duckout(i,1)=sin(atan(temp(i,1)/factor)/2)*q1;
duckout(i,2)=temp(i,2)/time;
end;
axis('normal');
plot(duckout(:,1), duckout(:,2), duckout(:,1), duckout(:,2),'o');
ylabel('I');
xlabel('Q  (A^-1)');
end
```

```
       PROGRAM readbinary
       CHARACTER infl*80,inf2*80
       INTEGER d(512),er,i,k1,hd(256),pmin,pmax
       INTEGER*2 itg(512)
       er=0
 1     print'(5x,a)','Raw data file ? '
       print*, 'HAVE YOU SAVED DATA FILE  SAVE -w  ?? '
       read(5,'(a)') infl
       if (er.eq.1) goto 1
       print' (5x,a)','Output data file ? '
       read(5,' (a)') inf2
       open(10,file=infl,status='old',access='direct',recl=1024)
       open(11,file=inf2,status='new',access='sequential')
* Read header of 1024 byte
       read(10,rec=1) (hd(i),i=1,256)
       print*,'Enter min then max  pixel'
       read(*,300) pmin
       read(*,300) pmax
 300   format(I4)
* Read 512 x 512 x 2 byte of data
       do 10 i=pmin,pmax
         k1=0
         read(10,rec=i+1) (itg(j),j=1,512)
         print*,i
         do 20 j=pmin,pmax
           if (itg(j).lt.0) then
             d(j)=0
           else
*  Divide intensity by 15 (less noise)
             d(j)=itg(j)/15
           endif
           k1=k1+d(j)
 20     continue
          if (k1 .eq. 0) then
          write(11,200) 9999
          else
* Write to file from 140 to 360
           do 30 kk=pmin,pmax
          write(11,200)itg(kk)
30       continue
          endif
10      continue
       close(10)
       close(11)
200    format(I5)
        end
```

```
function [outd,outds,x2,y2]=detectorread(tst,start,end);
% *************     DETECTORREAD   ****************
%  [outd,outds,x2,y2]=detectorread(tst,start,end);
% reads and plots on a 3-D graph the output of the detector screen
% run "readbinary" in SAXS and then transfer file
% tst is filename Assume start=140 end=360 221 points only
% Also smooths data and takes off beamstop points
%
% Outputs:  outd= 2-d original data, outds smoothed data -beamstop
%
% LAST MODIFIED: 9/15/93
% WRITTEN BY: Peter Kofinas

% Create 2-D matrix outd(x,y) from tst
le=length(tst);
nn1=end-start+1;
outd=zeros(nn1,nn1);
r=1;  % rows of output matrix
i=1;  % count for original file
tttt=' Reading file.  Be patient...'
while i <= le;
     if tst(i) ==9999;
        c=1;
        for k=1:nn1;
          outd(r,k)=1;
        end;
        r=r+1;
        i=i+1;
     else
      for j=1:nn1;
        outd(r,j)=tst(i);
        i=i+1;
      end;
      r=r+1;
     end;
end;

%Take off beamstop junk points, smooth  and plot final results
clc
clf reset
centerx=input('Center x of Data? ');
centery=input('Center y of Data? ');
r=input('Radius of Beamstop? ');
tttt=' Deleting Beamstop data ...'
outdb=beamstop(outd,centerx,centery,r,start);
tttt='Finally... Smoothing data'
[outds,x2,y2]=spline2dfit(outdb,start,end);
h=surfl(outds);
gg=input('Delete More beamstop data?  (1=yes) ');
if(gg==1)
  clf reset;
  etick=round(nn1/2);
  xx=1:etick;
  contour(xx,xx,outds');
  grid on;
  set(gca,'Xtick',1:5:etick);
  set(gca,'Ytick',1:5:etick);
  vec=input('Type in the coordinate range [x1 x2 y1 y2] ');
  outds(vec(1):vec(2),vec(3):vec(4))=zeros(vec(2)-vec(1)+1,vec(4)-vec(3)+1);
end;
```

************* DETECTORREAD ****************

```
clf reset;
grid off;
h1=surfl(x2,y2,outds);
orient landscape;
shading interp;


set(gca,'Visible','off');
colormap(gray);
brighten(-0.25);
end
```

```
function [outs,x2,y2]=spline2dfit(z,start1, end1);
% ****************   SPLINE2DFIT   *******************
% [outs,x2,y2]=spline2dfit(z,start1,end1) nn=rank=4 cubic
% out =512 x 512 detector output factor=2 for 111 x111, 1 otherwise
% modified from start1=140 to end1=360 currently
% start  and end1
% outs.mat smoothed output,  postscript
%
% Last Modified: 10/29/93
% Written by:  Peter Kofinas

nn=4;
le=length(z);
outs=zeros(le,le);
low=start1;
high=end1;
x=low:high;
y=low:high;
ky = nn;
vector=[low:4:high];
knotsy = augknt(vector,ky);
sp=spap2(knotsy,ky,y,z);
[ignored,coefsy]=spbrk(sp);
kx = nn;
knotsx=augknt(vector,kx);
sp2=spap2(knotsx,kx,x,coefsy');
[ignored,cxy]=spbrk(sp2);
coefs=cxy';
xv=low:2:high;
yv=low:2:high;
outs = fnval(spmak(knotsx,fnval(spmak(knotsy,coefs),yv)'),xv)';
[x2,y2]=meshgrid(xv,yv);
le=length(outs);
for i=1:le;
for j=1:le;
if(outs(i,j) < 0);
 outs(i,j)=0;
end;
end;
end;
end
```

```
% ****************BEAMSTOP *******************
% z=beamstop(z,centerx,centery,r,start2)
% Run this after DETECTORREAD
% z=detector matrix, c=center r=radius (integer pixels)
% Deletes beamstop points stores again in z
%
% LAST MODIFIED 10/28/93
% WRITTEN BY: PETER KOFINAS

lee=length(z);  outb=zeros(lee,lee);
shift=start2-1;
centerx=centerx-shift;  centery=centery-shift;
for i=1:rad;
     for k=0:90;
          xx=round(i*sin(k*pi/180));
          yy=round(i*cos(k*pi/180));
          da(1)=z(xx+centerx, yy+centery);
          da(2)=z(xx+centerx, -yy+centery);
          da(3)=z(-xx+centerx, -yy+centery);
          da(4)=z(-xx+centerx, yy+centery);
          if max(da) > 800
               da2(i)=max(da);
          else
               da2(i)= 800;
          end;
          z(xx+centerx, yy+centery)=0;
          z(xx+centerx, -yy+centery)=0;
          z(-xx+centerx, -yy+centery)=0;
          z(-xx+centerx, yy+centery)=0;
     end;
end;
% Now delete even more beamstop points
dd=min(da2);
for i=rad+1:rad+45;
     for k=1:90;
          xx=round(i*sin(k*pi/180));
          yy=round(i*cos(k*pi/180));
          if (xx+centerx >=lee | xx+centery >=lee)
            break;
          end;
          if z(xx+centerx, yy+centery) >= dd
            for j=-4:4;
               z(xx+centerx+j, yy+centery+j)=0;
            end;
          end;
          if z(xx+centerx, -yy+centery) >= dd
            for j=-4:4;
               z(xx+centerx+j, -yy+centery+j)=0;
            end;
          end;
          if z(-xx+centerx, -yy+centery) >= dd
            for j=-4:4;
               z(-xx+centerx+j, -yy+centery+j)=0;
            end;
          end;
          if z(-xx+centerx, yy+centery) >= dd
            for j=-4:4;
               z(-xx+centerx+j, yy+centery+j)=0;
            end;
          end;
     end;
end;
end
```

C.2 Permeability Programs

```
function err = fitfun(lambda)
% ********************** MYFITT4 *************************
% FITFUN Used by FITDEMO.
%       FITFUN(lambda) returns the error between the data and the
%       values computed by the current function of lambda.
%       FITFUN assumes a function of the form
%
%         y =  c(1)*exp(-lambda(1)*t) + ... + c(n)*exp(-lambda(n)*t)
%
%       with n linear parameters and n nonlinear parameters.
%
%  MODIFICATION OF EXISTING MATLAB ROUTINE FOR PERMEABILITY PROGRAMS
%  LAST MODIFIED: 4/2/93
%  MODIFIED BY: PETER KOFINAS

global Data t tt1 y lambda zz1
t = Data(:,1);
y = Data(:,2);
A = zeros(length(t),length(lambda));
for j = 1:size(lambda)
   A(:,j) = exp(-lambda(j)*t);
end
c = A\y;
z = A*c;
err = norm(z-y)
%hb=c(1)*exp(-lambda(1))+c(2)*exp(-lambda(2));
%hi=c(1)+c(2);
zz1= c(1)*exp(-lambda(1)*tt1)+ c(2)*exp(-lambda(2)*tt1);
axis([0,1,min(zz1)-2,max(zz1)+4]);
```

```
% ******************** FITRANDPERM ************************
% Fit random permeability data Setup for: METHANE
%
% LAST MODIFIED : 4/2/93
% WRITTEN BY: PETER KOFINAS

clg;
clear global;
clear;
x=[0, 0.349, 0.385, 0.556, 0.652, 0.745];
%x=[0 ,0.349, 0.556, 0.652, 0.745];
yco2=[116.537, 72.7, 51.8, 45.45, 38.95, 36.6];
yhe=[78.117, 33.5, 32, 18.1, 16.75, 13.6];
yy=[29.19, 13.5, 16.4, 9.35, 12.55, 8.7];
yo2=[37.452,16.5, 13.4, 9.75, 11.35, 7.8];
yn2=[26.045, 3.9, 3.65, 2.95, 1.9];
for i=1:6;
Data(i,1)=x(i);
Data(i,2)=yy(i);
end;
tt1=(0:0.01:1);
hold on
axis('square');
lam= [1 0]';
trace = 0;
tol = .1;
global Data  t tt1 y lambda zz1
lambda=fmins('myfit4',lam, [trace tol]);
% Statements to plot progress of fitting:
t=[ 0    0.3490    0.3850    0.5560    0.5560    0.6520    0.6520 0.745];
y=[29.19, 13.5, 16.4, 9.9, 8.8, 14.5, 10.6, 8.7];
plot(tt1,zz1, t, y, 'o');
save methane tt1 zz1 t y
title('Methane');
ylabel('P  barrers');
xlabel('% E');
hold off
echo off
```

```
function peff= ranfps(hb,hi,xb,f1,n);
% ******************** RANFPS ********************************
% peff=ranfps(hb,hi, f1, n), f1 from randomize
% Calculates effective permeability of random sample from permeability
% of components hb, hi  Assumes n x n grid
%
% LAST MODIFIED: 6/18/93
% WRITTEN BY: PETER KOFINAS

out1=zeros(n,1);
par3=zeros(n,1);
xi=1-xb;
par=xb*hb+xi*hi;
ser=1/(xb/hb+xi/hi);
sern=ser/n;
 for j=1:n;
  for i=1:n;
  k=f1(i,1);
  l=f1(j,2);
  cth=cos(se2(k,l)*pi/2);
   out=par*cth/n;
   if out < sern;
       out=sern;
   end;
    out1(i)=1/out;
  end;
   par2=mean(out1);
    par3(j)=1/par2;
end;
peff=sum(par3);
end



function cth=makepgrid(f1,n);
% ******************** MAKEPGRID **************************
% Makes random n x n grid for permeability calculations
% f1 from randomize
%
% LAST MODIFIED: 3/23/93
% WRITTEN BY: PETER KOFINAS

cl1=clock;
cl2=cl1(6)*rand*1000;
rand('uniform');
rand('seed',cl2);
cth=zeros(n,n);
se2=rand(n,n);
 for j=1:n;
  for i=1:n;
  k=f1(i,1);
  l=f1(j,2);
  cth(i,j)=cos(se2(k,l)*pi/2);
end;
end;
save cth.mat cth;
end
```

```
function peff= ranfps(hb,hi,xb);
% *****************  PPARFIT **********************
% peff= ranfps(hb,hi,xb);
% Caclulates paralel and series Permeability from component
%permeability data
%
% LAST MODIFIED:  2/15/93
% WRITTEN BY: PETER KOFINAS

xi=1-xb;
par=xb*hb+xi*hi
ser=1/(xb/hb+xi/hi)
end
```

```
function f1= randomize(n);
% *************** RANDOMIZE **********************
%f1=randomize(n), for n x n point grid
% Used to make a random grid for permeation calculations
%
% LAST MODIFIED : 6/17/93
% WRITTEN BY : PETER KOFINAS

rand('uniform');
vec1=zeros(10*n,1);
f1=zeros(n+1,2);
for j=1:2;
m=1;
vec1=round(n*rand(10*n,1));
     for i=1:10*n;
          vec2=vec1(i);
          if vec2==0;
               vec2=1;
          end;
          xend=find(f1(1:m,j)==vec2);
          if size(xend)==0;
               f1(m,j)=vec2;
               m=m+1;
          end;
          clear xend
     end;
end;
save f1.dat f1 /ascii;
end
```

Bibliography

[1] Haggin, J. *Chem. Eng. News* **1988**, 66(23),7.

[2] *Polymer Permeability*; Comyn, J., Ed; Elsevier Applied Science: London, 1985.

[3] Spillman, R. W. *Chem. Eng. Prog.* **1989**, *1*,41.

[4] Csernica, J.; Baddour, R. F.; Cohen, R. E. *Macromolecules* **1989**, *22*, 1493.

[5] Csernica, J.; Baddour, R. F.; Cohen, R. E. *Macromolecules* **1987**, *20*, 2468.

[6] Csernica, J.; Baddour, R. F.; Cohen, R. E. *Macromolecules* **1990**, *23*, 1429.

[7] Douzinas, K. C.; Cohen, R. E. *Macromolecules* **1992**, *25*, 5030.

[8] Cohen, R. E.; Bellare, A.; Drzewinski, M. A. *Macromolecules*, submitted.

[9] Almdal, K.; Koppi, K. A.; Bates, F. S. *Macromolecules* **1992**, *25*, 1743.

[10] Koppi, K. A.; Tirrell, M.; Bates, F. S. *Phys. Rev. Lett.* **1993**, *70(10)*, 1449.

[11] Koppi, K. A.; Tirrell, M.; Bates, F. S.:, Almdal, K.; Colby, R.H. *Journal De Physique II* **1993**, *2(11)*, 1941.

[12] Mohajer, Y.; Wilkes, G. L., Wang, J. E.; McGrath, J. E. *Polymer* **1982**, *23*, 1523.

[13] Seguela, R.; Prud'homme, J., *Polymer*, **1989**, *30* 1446.

[14] Rangarajan, P. Register, R. A.; Fetters, L. J.; *Macromolecules* **1993**, *26*, 4640.

[15] Hasegawa, H.; Tanaka, H.; Yamasaki, K.; Hashimoto, T. *Macromolecules* **1987**, *20*, 1651.

[16] Thomas, E.L.; Alward, D.B.; Kinning, D.L.; Martin, D.L.; Handlin, D.L.,Jr.; Fetters, L.J. *Macromolecules* **1986**, *19*, 2197.

[17] Hamley, I.W.; Koppi, K.A.; Rosedale, J.H.; Bates, F.S *Macromolecules* **1993**, *26*, 5959.

[18] Fredrickson, G.H.; Helfand, E.J. *J. Chem. Phys.* **1987**, *87*, 697.

[19] Roe, R.Y.; Fishkis, M.; Chang, J.C. *Macromolecules* **1981**, *14*, 1091.

[20] Hashimoto, T.; Tsukahara, Y.; Kawai, H. *J. Polym. Sci., Polym. Lett* **1980**, *18*, 585.

[21] Hashimoto, T.; Tsukahara, Y.; Kawai, H. *Macromolecules* **1981**, *14*, 708.

[22] Han, C.D.; Baek, D.M.; Kim, J.K. *Macromolecules* **1990**, *23*, 561.

[23] Koberstein, J.T.; Russell, T.P.; Walsh, D.J.; Pottick, L. *Macromolecules* **1990**, *23*, 877.

[24] Agawal, S., Ed. *Block Copolymers*; Plenum Press: New York, 1970.

[25] Helfand, E. *Macromolecules* **1975**, *8*, 552.

[26] Helfand, E.; Wasserman, Z.R. *Macromolecules* **1976**, *9*, 879.

[27] Helfand, E.; Wasserman, Z.R. *Macromolecules* **1978**, *11*, 960.

[28] Helfand, E.; Wasserman, Z.R. *Macromolecules* **1980**, *13*, 994.

[29] Noolandi, J.; Hong, K.M. *Ferroelectrics* **1980**, *30*, 117.

[30] Hong, K.M.; Noolandi, J. *Macromolecules* **1981**, 14, 727.

[31] Noolandi,J.; Hong, K.M *Macromolecules* **1982**, *15*, 482.

[32] Leibler, L. *Macromolecules* **1980**, *13*, 1602.

[33] Landau, L.D.; Lifshitz, E.M. *Statistical Physics*; Pergamon Press: Oxford, 1980; Part 1.

[34] de Gennes, P.-G. *J. Phys. (Paris)* **1970**, *31*, 235.

[35] Brazovskii, S.A. *Sov. Phys. -JETP (Engl. Transl.)* **1979**, 91, 7228.

[36] Mayes, A.M.; Olvera de la Cruz, M.J. *J. Chem. Phys.* **1991**, *95*, 4670.

[37] Mayes, A.M.; Olvera de la Cruz, M.J. *Macromolecules* **1991**, *24*, 3975.

[38] Mayes, A.M.; Olvera de la Cruz, M.J. *J. Chem. Phys.* **1989**, *91*, 7228.

[39] Bates, F.S.; Rosedale, J.H.; Fredrickson, G.H.; Glinka, C.J. *Phys. Rev. Lett.* **1988**, *61*, 2229.

[40] Keller, A.; Pedemonte, E; Willmouth, F.M. Colloid Polym. Sci. **1970**, *238*, 385.

[41] Hadziioannou, G.; Mathis, A.; Skoulios, A. *Colloid Polym. Sci.* **1979**, *257*, 136.

[42] Morrison, F.; Bourvellec, G.L.; Winter, H.H. *J. Appl. Polym. Sci.* **1987**, *33*, 1585.

[43] Winey, K.L.; Patel, S.S.; Larson, R.G.; Watanabe, H. *Macromolecules* **1992**, *25*, 4175.

[44] Cohen, R.E.; Bates, F.S.; *J. Polym. Sci., Polym. Phys. Ed.* **1980**, *18*, 2143.

[45] Whitmore, M.D.; Noolandi, J. *Macromolecules* **1988**, *21*, 1482.

[46] Douzinas, K. C.; Cohen, R. E.; Halasa, A. F. *Macromolecules* **1991**, *24*, 4457.

[47] Aminabhavi, T.M.; Aithal, U.S.; Shukla, S.S. *J. Macrom. Sci-Rev. Macrom. Chem. Phys.* **1988**, *C28(3-4)*, 421.

[48] Csernica, J.J. 'Gas Permeation in Block Copolymer Films', Ph.D. Thesis, Massachusetts Institute of Technology, Cambridge, MA, 1989.

[49] Rein, D.H. 'The Control of Gas Transport in Heterogeneous Polymer Systems', Ph.D. Thesis, Massachusetts Institute of Technology, Cambridge, MA, 1991.

[50] Halasa, A. F. U.S. Patent 3 872 072.

[51] Cohen, R. E.; Cheng, P.-L.; Douzinas, K.; Kofinas, P.; Berney, C. V. *Macromolecules* **1990**, *23*, 324.

[52] Lin, L; Argon, A. S. *Macromolecules* **1992**, *25*, 4011.

[53] Song, H. H; Argon, A. S.; Cohen, R. E. *Macromolecules* **1990**, *23*, 870.

[54] Galeski, A.; Argon, A. S.; Cohen, R. E. *Macromolecules* **1992**, *25*, 5705.

[55] Gray, R. W.; Young, R. J., *J. Mater. Sci* **1974**, *9*, 521.

[56] ASTM D-1434, American Society for Testing and Materials: Philadelphia, 1984.

[57] Spruiell, J. E.; Clark, E. S. *Methods of Experimental Physics*; Academic Press: New York, 1980; Vol. 16B, Chapter 6.

[58] Song, H. H.; Argon, A. S.; Cohen, R. E. *Macromolecules* **1990**, *23*, 870.

[59] Bates, F. S.; Schultz, M. F.; Rosedale, J. H. *Macromolecules* **1992**, *25*, 5547.

[60] Michaels, A. S.; Vieth, W. R.; Barrie, J. A. *J. Appl Phys.* **1963**, *34(1)*, 1.

[61] Mohr, J. M.; Paul, D. R. *J. Appl. Pol. Sci.* **1991**, *42*, 1711.

[62] Pauly,S.; in "Polymer Handbook", 3rd ed., eds Brand, J. and Immergut, E. H., Wiley, New York, 1989.

[63] van Amerongen, G. J. *J. Appl. Phys.* **1946**, *17*, 972.